

Initialization with a Fock State Cavity Mode in Real-Time Nuclear–Electronic Orbital Polariton Dynamics

Millan F. Welman and Sharon Hammes-Schiffer

Department of Chemistry, Princeton University, Princeton, NJ 08544

Molecular polaritons have drawn great interest in recent years as a possible avenue for providing optical control over chemical dynamics. A central challenge in the field is to identify physical phenomena that require a quantum rather than a classical treatment of electrodynamics. In this work, we use our recently developed mean-field quantum (mfq) and full-quantum (fq) real-time nuclear–electronic orbital (RT-NEO) time-dependent density functional theory methods to simulate polaritonic dynamics for a molecule under vibrational strong coupling when a quantized cavity mode is initialized in a Fock state rather than a coherent state. Our previous work showed that a coherent state initial condition for the cavity mode leads to polariton formation for both the mfq-RT-NEO and fq-RT-NEO methods. Herein, we show that the mfq-RT-NEO method, which does not allow light–matter entanglement, does not predict polariton formation for a Fock state initial condition. Similar to the mfq-RT-NEO method, the fq-RT-NEO method does not predict oscillations of the cavity mode coordinate and molecular dipole operator expectation values for a Fock state initial condition. However, the fq-RT-NEO method does predict oscillations of the expectation values of even powers of these operators as well as light–matter entanglement, implicating polariton formation with a Fock state initial condition. All these observations can be explained with model systems. These results suggest that using a quantized cavity mode initial condition that does not have a direct analogy to an initial condition in classical electrodynamics can lead to physical phenomena that can only be described by a quantum treatment of the cavity mode.

I. INTRODUCTION

Molecular polaritons are quasiparticles formed by strong coupling between light and matter degrees of freedom.¹ When an incident electromagnetic field interacts with a system of one or more molecules, it induces an oscillation in the charge distribution of the molecular system. The oscillating molecular charge distribution in turn generates another electromagnetic field, which can interact with and alter the behavior of the incident field that created it. This feedback cycle will occur if the dissipation timescale of the incident field is comparable to or much slower than the timescale of energy exchange between the molecular system and the electromagnetic field.² This phenomenon can be realized experimentally in settings such as plasmonic nanocavities,³ where a small number of molecules interact with a plasmonic mode, or Fabry-Pérot optical cavities,^{4,5} where a large number of molecules is confined between two mirrors and allowed to interact with cavity modes bounded by the mirrors. The total light–matter system is said to be under electronic strong coupling (ESC)^{6,7} when the electromagnetic mode is coupled to an electronic transition and under vibrational strong coupling (VSC)^{8–10} when the electromagnetic mode is coupled to a vibrational transition.

Recent experimental data suggest that strong light–matter coupling may be used to modify chemical dynamics ranging from energy transfer and exciton transport processes^{11–20} to reaction rates^{21–23} and branching ratios.²⁴ This experimental progress in turn has spurred the development of a variety of theoretical methods ranging from canonical quantum optics models^{25–27} to quantum-electrodynamical (QED) electronic structure methods,^{28–36} which have shed light on the nature of polaritonic stationary states and the dynamics of polaritonic model systems. Among theoretical methods for simulating molecular polaritons, dynamical methods provide a unique perspective by capturing the feedback between light and matter in real

time. An important consideration is whether the electromagnetic field should be treated classically or quantum mechanically. Either choice can be used to simulate polariton dynamics because the feedback between light and matter is predicted by both classical and quantum electrodynamics. Each approach has its own distinct advantages.

Semiclassical treatments of light–matter interactions, where a classical electromagnetic field is coupled to a quantum mechanical matter system, have found widespread applications in the study of problems ranging from weak to strong light–matter coupling.^{37–44} Indeed, a semiclassical method often constitutes the only computationally feasible approach to simulating the collective strong light–matter coupling that occurs experimentally in a Fabry–Pérot cavity. The cavity molecular dynamics (CavMD) method⁴⁵ provides such a framework for carrying out computationally tractable simulations of collective strong coupling under VSC. CavMD simulations have thus far yielded significant insights into relaxation and energy transfer processes in non-reactive dynamics under VSC.^{46–49} In addition to the extensive theoretical literature employing semiclassical methods, it is well-known experimentally that classical transfer matrix methods accurately predict polaritonic absorption lineshapes in the limit of a large molecular ensemble, as would occur in a Fabry–Pérot cavity.⁵⁰ This result has recently been verified analytically,⁵¹ suggesting that a semiclassical treatment may provide an acceptable description of light–matter interactions under collective strong coupling.

In contrast to the semiclassical treatment, a fully quantum mechanical approach that features a quantized electromagnetic field allows for the inclusion of effects such as light–matter entanglement and spontaneous emission. Such a treatment may be computationally feasible for a system composed of a few molecules, as realized experimentally in a plasmonic nanocavity.^{4,5} Further motivation for a fully quantum mechanical treatment is provided by recent model system studies suggesting that

there may be limitations to the semiclassical treatment of polariton dynamics.^{52–59} Therefore, it is of great importance to better understand the potential limitations of a semiclassical treatment relative to a fully quantum mechanical treatment and how those limitations may manifest in dynamical simulations of polaritons.

To address this challenge, we recently developed a hierarchy of first-principles dynamical simulation methods for molecular polaritons.^{60,61} These methods treat the molecular system with real-time nuclear–electronic orbital time-dependent density functional theory (RT-NEO-TDDFT, hereafter RT-NEO).⁶² The RT-NEO method is the extension of conventional electronic RT-TDDFT to the NEO framework. In the NEO framework,^{63,64} specified nuclei, usually protons, are treated quantum mechanically on the same footing as the electronic degrees of freedom. The RT-NEO method provides an approach for the propagation of nonequilibrium molecular quantum dynamics that incorporates zero-point energy, tunneling, proton delocalization, and other nuclear quantum effects. Coupling molecular dynamics propagated with RT-NEO to the dynamics of a cavity mode thus provides a first-principles route to simulating polariton dynamics under VSC that incorporates nuclear quantum effects. In this work, we will utilize two of the three methods in this hierarchy, omitting the semiclassical method, which treats the cavity mode classically.

Both RT-NEO methods that we will use in this work treat the cavity mode quantum mechanically but differ in their treatment of light–matter entanglement. The mean-field-quantum RT-NEO (mfq-RT-NEO) method self-consistently propagates separate equations of motion for the molecular density matrix and the cavity mode density matrix. The two density matrices are coupled to each other through the expectation values of the cavity mode coordinate operator and the molecular dipole operator. This treatment is equivalent to assuming that there is no quantum entanglement between the molecular system and the cavity mode. In contrast to the mfq-RT-NEO method, the full-quantum RT-NEO (fq-RT-NEO) method allows for

light-matter entanglement by propagating a joint light-matter density matrix that describes both the molecular and cavity mode degrees of freedom. In Ref. 61, we used these methods to study non-reactive single-molecule polariton dynamics for the HCN molecule under vibrational strong coupling, where all electrons and the hydrogen nucleus are treated quantum mechanically. Under a consistent set of initial conditions, these two methods yielded excellent agreement in their description of the oscillations of the quantum nuclear dipole moment. The dynamics of the light-matter entanglement computed with the fq-RT-NEO method, however, revealed a new oscillation timescale absent from the mfq-RT-NEO results. This finding suggested that new physics might be uncovered by considering the role of light-matter entanglement.

The mfq-RT-NEO and fq-RT-NEO simulations in our previous work used a common set of initial conditions. The HCN molecular system was initialized in its ground state, while the cavity mode was initialized in a coherent state with a nonzero coordinate expectation value. This choice was made because coherent states provide an ideal initial condition for methods with a quantum cavity mode to enable a direct comparison to the results of semiclassical methods with a classical cavity mode. In the absence of light-matter coupling, the expectation values of the coordinate and momentum operators of a quantum cavity mode initialized in a coherent state will oscillate harmonically like a classical cavity mode. It is straightforward, however, to choose initial quantum mode conditions that do not lead to classical-like oscillations in the absence of light-matter coupling. The most obvious example of this is a Fock (number) state, or a quantum harmonic oscillator eigenstate, where the number of the state corresponds to the integer number of photons populating the cavity mode. This initial condition is of interest because it corresponds to the traditional model understanding of polaritons, where the cavity mode is populated with a single photon, and the photon is then exchanged coherently with a molecular system. Unlike a classical harmonic oscillator, a quantum harmonic oscillator in a Fock state

can simultaneously have a nonzero energy expectation value and zero position and momentum expectation values.⁶⁵ This insight suggests that more significant deviations from the general qualitative features of semiclassical polariton dynamics may be found if the quantum mode is initialized in a Fock state.

The goal of this paper is to perform m fq-RT-NEO and f q-RT-NEO simulations of single-molecule polariton dynamics with a quantum cavity mode initialized in a Fock state and to determine if these dynamics exhibit qualitatively new features that do not occur in polariton dynamics where the cavity mode is treated classically or quantum mechanically with a coherent state initial condition. The paper is organized as follows. In section 2, we review the theory of m fq-RT-NEO and f q-RT-NEO, as well as our procedure for computing light–matter entanglement. Simulation details for HCN under vibrational strong coupling are provided in section 3. In section 4, we present the results of the m fq-RT-NEO and f q-RT-NEO calculations. Finally, section 5 provides a more detailed analysis of our results, aided by comparison to quantum optics models. Conclusions are provided in section 6.

II. THEORY

In this section, we provide an overview of the m fq-RT-NEO and f q-RT-NEO methods. The interested reader is referred to Ref. 61 for a more detailed derivation and discussion of these methods.

Our starting point is the QED Hamiltonian written in the long-wavelength approximation:

$$\hat{H}_{\text{QED}} = \hat{H}_{\text{M}} + \sum_{k,\lambda} \left[\frac{1}{2} \hat{p}_{k,\lambda}^2 + \frac{1}{2} \omega_{k,\lambda}^2 \left(\hat{q}_{k,\lambda} + \frac{\hat{\mu}_{\text{M}} \cdot \boldsymbol{\xi}_{\lambda}}{\omega_{k,\lambda} \sqrt{\Omega \epsilon_0}} \right)^2 \right] \quad (1)$$

where \hat{H}_M is the molecular Hamiltonian,

$$\hat{H}_M = \sum_i \left(\frac{\hat{\mathbf{p}}_i^2}{2m_i} + \hat{V}(\{\hat{\mathbf{r}}_i\}, \{\mathbf{R}_c\}) \right) \quad (2)$$

The summation with index i runs over all quantum mechanical particles (i.e., electrons and specified quantum nuclei for NEO methods). The operator $\hat{V}(\{\hat{\mathbf{r}}_i\}, \{\mathbf{R}_c\})$ includes all Coulomb interactions among quantum particles with coordinate operators $\{\hat{\mathbf{r}}_i\}$ and classical nuclei at fixed coordinates $\{\mathbf{R}_c\}$. The summation in Eq. 1 is over all cavity modes with wave vector magnitude $k = |\mathbf{k}| = \omega_{k,\lambda}/c$, where c is the speed of light, and polarization direction given by the unit vector ξ_λ . These two vectors are orthogonal, such that $\mathbf{k} \cdot \xi_\lambda = 0$. The operators $\hat{q}_{k,\lambda}$ and $\hat{p}_{k,\lambda}$ and the scalar $\omega_{k,\lambda}$ are the coordinate operator, momentum operator, and frequency, respectively, of a mode determined by the vectors \mathbf{k} and ξ_λ . The coordinate operator $\hat{q}_{k,\lambda}$ is coupled to the total molecular dipole moment $\hat{\mu}_M$. Finally, ϵ_0 is the permittivity of free space, and Ω denotes the effective volume of the cavity.

If we restrict our consideration to the strong coupling regime, avoiding the ultra-strong coupling regime, we can neglect the term in Eq. 1 that is quadratic in $\hat{\mu}_M$. We also assume that the total molecular density matrix $\mathbf{P}_{en}(t)$ can be written as a product of separate electronic and quantum nuclear density matrices:

$$\mathbf{P}_{en}(t) = \mathbf{P}_e(t) \otimes \mathbf{P}_n(t) \quad (3)$$

Introducing the subscript F (for “field”) to denote quantities defined in the cavity mode Hilbert space, we can express the fq-RT-NEO equations of motion for the joint density matrix $\mathbf{P}_{Fn}(t)$ describing the cavity mode and nuclear degrees of freedom and the density matrix $\mathbf{P}_e(t)$ describing the electronic degrees of freedom as

$$i\hbar \frac{\partial}{\partial t} \mathbf{P}_{Fn}(t) = \left[\mathbf{I}_F \otimes \mathbf{F}_n^{NEO}(t) + \mathbf{H}_F \otimes \mathbf{I}_n + \sum_{k,\lambda} \varepsilon_{k,\lambda} \mathbf{q}_{k,\lambda} \otimes (\boldsymbol{\mu}_{n,\lambda} - \mu_{n,\lambda}^0 \mathbf{I}_n), \mathbf{P}_{Fn}(t) \right] \quad (4)$$

$$i\hbar \frac{\partial}{\partial t} \mathbf{P}_e(t) = [\mathbf{F}_e^{\text{NEO}}(t), \mathbf{P}_e(t)] \quad (5)$$

Cavity mode and molecular operators are multiplied using the Kronecker product \otimes , which expands operators in the individual molecular and cavity mode Hilbert spaces into the joint molecule-mode Hilbert space. \mathbf{I}_F and \mathbf{H}_F are the matrix representations of the identity operator \hat{I}_F in the mode Hilbert space and the sum of harmonic oscillator Hamiltonians \hat{H}_F given by

$$\hat{H}_F = \sum_{k,\lambda} \left[\frac{1}{2} \hat{p}_{k,\lambda}^2 + \frac{1}{2} \omega_{k,\lambda}^2 \hat{q}_{k,\lambda}^2 \right] \quad (6)$$

In Eq. 4, $\mathbf{q}_{k,\lambda}$ is the matrix representation of $\hat{q}_{k,\lambda}$ defined above, and \mathbf{I}_n is the matrix representations of the identity operator \hat{I}_n in the molecular Hilbert space. The light-matter coupling $\varepsilon_{k,\lambda}$ between the molecular system and the mode $\{k, \lambda\}$ is

$$\varepsilon_{k,\lambda} = \frac{\omega_{k,\lambda}}{\sqrt{\Omega\epsilon_0}} \quad (7)$$

The matrix $\boldsymbol{\mu}_{n,\lambda}$ is the matrix representation of the single-particle quantum nuclear dipole moment operator's component in the polarization direction λ . We subtract the component of the permanent quantum nuclear dipole moment in the cavity mode direction, $\mu_{n,\lambda}^0$, from the dipole moment operator to ensure that the mode is not perturbed by the permanent dipole moment at $t = 0$.

The electronic and nuclear time-dependent Kohn-Sham matrices, $\mathbf{F}_e^{\text{NEO}}(t)$ and $\mathbf{F}_n^{\text{NEO}}(t)$, are given by

$$\mathbf{F}_e^{\text{NEO}}(t) = \mathbf{H}_{\text{core}}^e + \mathbf{J}^{\text{ee}}[\mathbf{P}_e(t)] + \mathbf{V}_{\text{xc}}^{\text{ee}}[\mathbf{P}_e(t)] - \mathbf{J}^{\text{en}}[\mathbf{P}_n(t)] - \mathbf{V}_{\text{c}}^{\text{en}}[\mathbf{P}_e(t), \mathbf{P}_n(t)] \quad (8)$$

$$\mathbf{F}_n^{\text{NEO}}(t) = \mathbf{H}_{\text{core}}^n + \mathbf{J}^{\text{nn}}[\mathbf{P}_n(t)] + \mathbf{V}_{\text{xc}}^{\text{nn}}[\mathbf{P}_n(t)] - \mathbf{J}^{\text{ne}}[\mathbf{P}_e(t)] - \mathbf{V}_{\text{c}}^{\text{ne}}[\mathbf{P}_n(t), \mathbf{P}_e(t)] \quad (9)$$

In Eq. 9, $\mathbf{H}_{\text{core}}^n$ is the core Hamiltonian describing the quantum nuclear kinetic energy and the Coulomb interaction between quantum and classical nuclei; $\mathbf{J}^{\text{nn}}[\mathbf{P}_n(t)]$ describes the Coulomb interaction between quantum nuclei; $\mathbf{V}_{\text{xc}}^{\text{nn}}[\mathbf{P}_n(t)]$ describes the

exchange-correlation interaction between quantum nuclei; $\mathbf{J}^{\text{ne}}[\mathbf{P}_e(t)]$ describes the Coulomb interaction between quantum nuclei and electrons; and $\mathbf{V}_c^{\text{ne}}[\mathbf{P}_n(t), \mathbf{P}_e(t)]$ describes the correlation energy between quantum nuclei and electrons. The electronic quantities in Eq. 8 are defined analogously.

Note that the cavity mode only couples directly to the quantum nuclear dipole moment and does not couple directly to the electronic dipole moment. This approximation is justified if the electronic and vibrational transitions correspond to significantly different energy scales, and the cavity mode energy corresponds to vibrational excitations. Thus, this approximation is reasonable for VSC on the ground-state electronic surface, where infrared radiation probes vibrational polaritons. The cavity modes are coupled indirectly to the electronic degrees of freedom through the dependence of the electronic and nuclear time-dependent Kohn-Sham matrices on both the electronic and quantum nuclear density matrices, $\mathbf{P}_e(t)$ and $\mathbf{P}_n(t)$.

To compute observables for either the cavity mode or quantum nuclear subsystems, we can take the partial trace of the joint density matrix $\mathbf{P}_{Fn}(t)$ over the degrees of freedom of the other subsystem to obtain

$$\mathbf{P}_n(t) = \text{Tr}_F[\mathbf{P}_{Fn}(t)] \quad (10)$$

$$\mathbf{P}_F(t) = \text{Tr}_n[\mathbf{P}_{Fn}(t)] \quad (11)$$

To measure the light-matter entanglement, we compute the von Neumann entropy $S(t)$, given by

$$S(t) = -\text{Tr}[\mathbf{P}_n(t) \ln \mathbf{P}_n(t)] = -\text{Tr}[\mathbf{P}_F(t) \ln \mathbf{P}_F(t)] \quad (12)$$

The second equality is proved in the Supporting Information of Ref. 61 and has been confirmed numerically for our simulations. In our code, we compute $S(t)$ using $\mathbf{P}_n(t)$. $S(t)$ has a minimum value of 0, corresponding to the case where $\mathbf{P}_{Fn}(t)$ is separable into cavity mode and quantum nuclear density matrices. The von Neumann entropy

quantifies how close $\mathbf{P}_{Fn}(t)$ is to being separable. A larger value of $S(t)$ means that $\mathbf{P}_{Fn}(t)$ is further from being separable. The maximum possible value of $S(t)$ in a simulation is $S_{\max} = \ln(N_{\min})$, where N_{\min} is the smaller of the cavity mode and molecular basis set sizes. Other relevant properties of $S(t)$ are discussed in Ref. 61.

To obtain the mfq-RT-NEO equations of motion, we assume that the joint density matrix $\mathbf{P}_{Fn}(t)$ is separable at all times $t \geq 0$:

$$\mathbf{P}_{Fn}(t) = \mathbf{P}_F(t) \otimes \mathbf{P}_n(t) \quad (13)$$

This is equivalent to assuming that there is zero light-matter entanglement. Eq. 4 then separates into two coupled equations of motion, one for the cavity mode density matrix $\mathbf{P}_F(t)$ and the other for the quantum nuclear density matrix $\mathbf{P}_n(t)$. The equation of motion for the electronic density matrix $\mathbf{P}_e(t)$ given by Eq. 5 remains unchanged. The resulting equations of motion are

$$i\hbar \frac{\partial}{\partial t} \mathbf{P}_F(t) = \left[\mathbf{H}_F + \sum_{k,\lambda} \varepsilon_{k,\lambda} \mathbf{q}_{k,\lambda} \mu_{n,\lambda}(t), \mathbf{P}_F(t) \right] \quad (14)$$

$$i\hbar \frac{\partial}{\partial t} \mathbf{P}_n(t) = \left[\mathbf{F}_n^{\text{NEO}}(t) + \sum_{k,\lambda} \varepsilon_{k,\lambda} q_{k,\lambda}(t) \boldsymbol{\mu}_{n,\lambda}, \mathbf{P}_n(t) \right] \quad (15)$$

$$i\hbar \frac{\partial}{\partial t} \mathbf{P}_e(t) = [\mathbf{F}_e^{\text{NEO}}(t), \mathbf{P}_e(t)] \quad (16)$$

Here, $q_{k,\lambda}(t) \equiv \text{Tr}[\mathbf{P}_F(t) \mathbf{q}_{k,\lambda}]$ denotes the expectation value of $\hat{q}_{k,\lambda}$ at time t , and $\mu_{n,\lambda}(t) \equiv \text{Tr}[\mathbf{P}_n(t) \boldsymbol{\mu}_{n,\lambda}] - \text{Tr}[\mathbf{P}_n(0) \boldsymbol{\mu}_{n,\lambda}]$ denotes the expectation value of the time-dependent quantum nuclear dipole moment operator at time t minus the permanent dipole moment.

III. SIMULATION DETAILS

The fq-RT-NEO and mfq-RT-NEO methods are implemented in a developer version of QChem.⁶⁶ In the fq-RT-NEO method, all quantum mechanical degrees of

freedom (mode, quantum nuclei, and electrons) are propagated with a modified-midpoint unitary transform (MMUT) time-propagation scheme⁶⁷ with an additional predictor-corrector scheme⁶⁸ used to control numerical error during the real-time dynamics. The quantum molecular degrees of freedom in the mfq-RT-NEO method are propagated with the same scheme, while the quantum mode degrees of freedom are propagated with the time-evolution operator $\exp(-i\mathbf{H}t/\hbar)$, where $\mathbf{H} = \mathbf{H}_F + \sum_{k,\lambda} \varepsilon_{k,\lambda} \mathbf{q}_{k,\lambda} \mu_{n,\lambda}(t)$ with all terms defined above. The classical nuclei are fixed at specified geometries in both methods.

We simulated HCN under VSC with the electrons and the proton treated quantum mechanically. The calculations were performed with the cc-pVDZ⁶⁹ electronic basis set and the even-tempered 8s8p8d⁷⁰ protonic basis set with exponents ranging from $2\sqrt{2}$ to 32. The B3LYP⁷¹⁻⁷³ electronic exchange-correlation functional and the epc17-2^{70,74} electron-proton correlation functional were used. The C-N bond length was taken to be 1.16 Å, and the distance between the proton basis function center and the carbon nucleus was taken to be 1.07 Å. The cavity mode was described with four number basis functions $|i\rangle, i = 0, 1, 2, 3$, which is the largest computationally tractable basis set that can be used with the aforementioned molecular basis sets given our resources.

At $t = 0$ for the fq-RT-NEO method, we initialized the joint cavity mode–nuclear density matrix $\mathbf{P}_{Fn}(0)$ as a separable product of cavity mode and quantum nuclear density matrices: $\mathbf{P}_{Fn}(0) = \mathbf{P}_F(0) \otimes \mathbf{P}_n(0)$. We chose $\mathbf{P}_F(0) = |1\rangle\langle 1|$ (i.e., we initialized the cavity mode in the first harmonic oscillator excited state populated by a single photon), and we chose $\mathbf{P}_n(0)$ to be the self-consistent field (SCF) ground state quantum nuclear density matrix from a NEO-DFT calculation. We also chose $\mathbf{P}_e(0)$ to be the SCF ground state electronic density matrix from the same NEO-DFT calculation. Identical initial conditions were used for the mfq-RT-NEO calculation, with the only difference being that we did not need to initialize a joint mode–nuclear

density matrix because this method propagates those subsystems separately. We propagated the real-time dynamics with a time step of $\Delta t = 0.04$ a.u. and light-matter coupling of 8×10^{-4} a.u. for both methods. All power spectra $P\{f(t)\}$ of real-time data $f(t)$ were computed as $P\{f(t)\} = |\mathcal{F}\{f(t)e^{-\gamma t}\}|$, where $\mathcal{F}\{\dots\}$ denotes the Padé approximation^{68,75} to the Fourier transform. We used a small damping of $\gamma = 10^{-5}$ a.u., giving a linewidth of 1.7×10^{-3} eV = 13.8 cm^{-1} to all peaks.

IV. RESULTS

We consider the HCN molecule shown in Figure 1a. At $t = 0$, we initialize the molecule in its NEO-DFT ground state and populate the cavity mode with one photon, corresponding to initializing it in the first harmonic oscillator excited state or single-photon Fock state. The molecule is coupled to an x -polarized lossless cavity mode tuned to be in resonance with the x -direction bending mode of the quantum proton, which has frequency $\omega_c = 2803 \text{ cm}^{-1}$ at this level of theory, and the light-matter coupling strength is $\varepsilon = 8 \times 10^{-4}$ a.u. We then propagate the real-time excited state dynamics with either the mfq-RT-NEO or fq-RT-NEO method.

First we consider the results from the mfq-RT-NEO dynamics simulation. Figure 1a shows the time evolution of the cavity mode coordinate, $q(t) \equiv \text{Tr}[\mathbf{P}_F(t)\mathbf{q}_{k,x}] - \text{Tr}[\mathbf{P}_F(0)\mathbf{q}_{k,x}]$, and quantum nuclear dipole moment, $\mu_{n,x}(t) \equiv \text{Tr}(\mathbf{P}_n(t)\boldsymbol{\mu}_{n,x}) - \text{Tr}(\mathbf{P}_n(0)\boldsymbol{\mu}_{n,x})$, where k is the magnitude of the cavity mode wavevector as defined in the context of Eq. 1, and the cavity mode is polarized in the x -direction. Both quantities remain constant for the duration of the dynamics, suggesting that at the mfq-RT-NEO level of theory, energy exchange does not occur between the cavity mode and molecular subsystems when the mode subsystem is initialized in a Fock state and the molecule is initialized in its ground state. In other words, a molecular polariton is not formed because there is no feedback interaction between the two

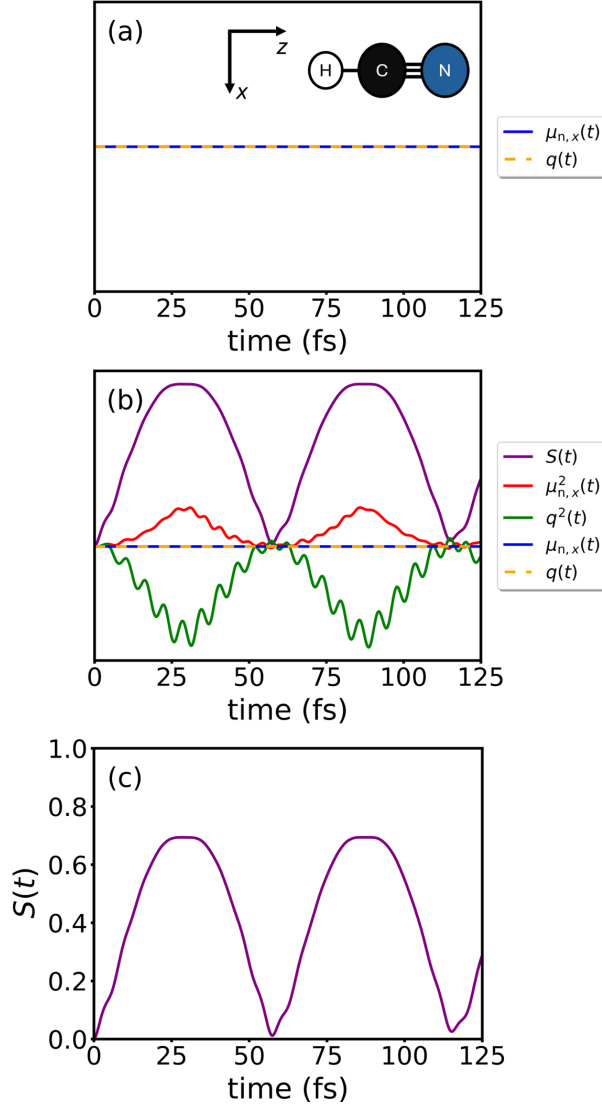


Figure 1. Comparison of time-dependent properties computed with mfq- and fq-RT-NEO dynamics applied to HCN. (a) mfq-RT-NEO dynamics of $\mu_{n,x}(t)$ and $q(t)$. No significant oscillations are observed. No units are given on the y -axis because these observables have different units. (b) fq-RT-NEO dynamics of $\mu_{n,x}(t)$ and $q(t)$, as well as $S(t)$, $\mu_{n,x}^2(t)$ and $q^2(t)$. No units are given on the y -axis because these observables have different units. (c) fq-RT-NEO dynamics of $S(t)$. The maximum computed value of $S(t)$ is ~ 0.67 .

subsystems. This result can be easily rationalized by considering the mfq-RT-NEO equations given by Eqs. 14 and 15. At $t = 0$, $\mu_{n,x}(t) = 0$, so according to Eq. 14, the field density matrix $\mathbf{P}_F(t)$ is unchanged. By the same reasoning, given that $q(t) = 0$ at $t = 0$, the quantum nuclear density matrix $\mathbf{P}_n(t)$ is also unchanged. Without a further perturbation, the density matrices are preserved, leaving all observables unchanged from their initial values. We note that a similar argument in the context of a model polaritonic system with a classical cavity mode was recently made in Ref. 57.

We now examine whether the absence of coherent molecule–mode energy transfer and polariton formation persists under fq-RT-NEO dynamics. Figure 1b shows the time evolution of $q(t)$, $\mu_{n,x}(t)$, and the von Neumann entropy $S(t)$. Once again, $q(t)$ and $\mu_{n,x}(t)$ remain essentially unchanged from their initial values. The persistence of this result is surprising given that neither $\hat{q}_{k,\lambda}$ nor $\hat{\mu}_{n,x}$ commute with \hat{H}_{QED} , and hence their expectation values are not expected to be constants of motion. These results will be considered in more detail in the Discussion.

In contrast, the von Neumann entropy $S(t)$ shows clear oscillations on a timescale of ~ 59 fs in the fq-RT-NEO dynamics. These oscillations are of significant amplitude. The maximum possible value of the von Neumann entropy that could be theoretically attained in this simulation is given by the natural logarithm of the smaller of the quantum nuclear and cavity mode basis sets. The cavity mode basis set is smaller with only four functions, so $S_{\text{max}} = \ln(4) = 1.38$. Figure 1c shows that the maximum value of $S(t)$ computed in the fq-RT-NEO calculation is ~ 0.67 , or approximately 48% of S_{max} . Although not a perfect comparison, it is still worth noting that this degree of light–matter entanglement is far larger than the degree of light–matter entanglement observed when the cavity mode was initialized in a coherent state with a small initial displacement in the linear response regime.⁶¹ This result suggests that coherent energy transfer between the molecule and cavity mode subsystems

may be occurring, even if the cavity mode coordinate and quantum nuclear dipole moment are constant throughout the dynamics. We hypothesized that this transfer process might manifest in oscillations of the expectation values of the operators $\hat{q}_{k,x}^2$ and $\hat{\mu}_{n,x}^2$. To interrogate this possibility, we also plot the dynamics of $q^2(t) \equiv \text{Tr}[\mathbf{P}_F(t)\mathbf{q}_{k,x}^2] - \text{Tr}[\mathbf{P}_F(0)\mathbf{q}_{k,x}^2]$ and $\mu_{n,x}^2(t) \equiv \text{Tr}[\mathbf{P}_n(t)\boldsymbol{\mu}_{n,x}^2] - \text{Tr}[\mathbf{P}_n(0)\boldsymbol{\mu}_{n,x}^2]$ in Figure 1b. Both quantities display slow oscillations, again on a timescale of ~ 59 fs, as well as fast oscillations on a timescale of ~ 6 fs. The fast oscillation timescale is almost exactly half of that corresponding to the oscillation frequency ω_c of the cavity mode, which is $2\pi/\omega_c \approx 12$ fs.

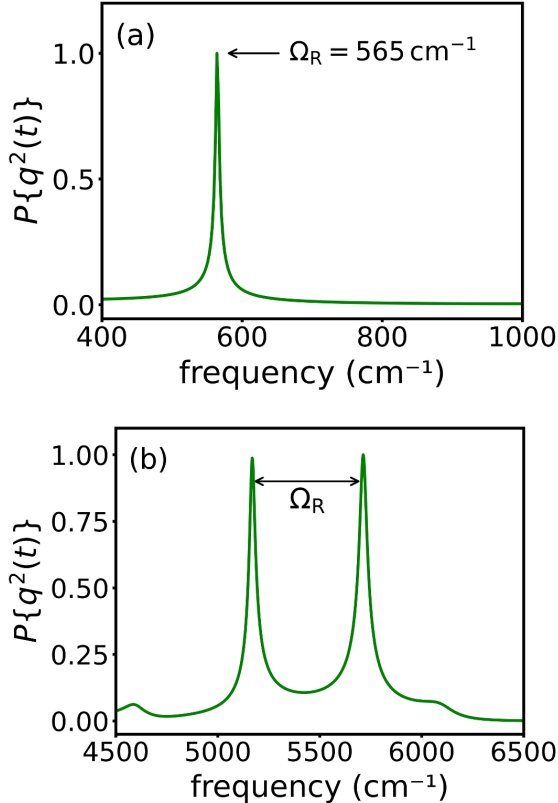


Figure 2. Power spectrum of $q^2(t)$ obtained with fq-RT-NEO dynamics applied to HCN for the (a) 400 - 1000 cm^{-1} region and (b) 4500 - 6500 cm^{-1} region. In both spectra, the largest signal amplitude has been scaled to a value of 1.

In order to quantify the frequencies more precisely, we considered the power spectrum of $q^2(t)$. Figure 2a shows the power spectrum of $q^2(t)$ in the spectral region of 400 to 1000 cm^{-1} , exhibiting a single peak at 565 cm^{-1} . This frequency corresponds to an oscillation timescale of 59 fs, matching the slow frequency observed in the oscillations of $S(t)$, $q^2(t)$, and $\mu_{n,x}^2(t)$. We will interpret this frequency as the Rabi frequency and denote it as Ω_R . Figure 2b shows the power spectrum of $q^2(t)$ in the spectral region of 4500 to 6500 cm^{-1} . The power spectrum in this region shows a pair

of peaks centered at 5437 cm^{-1} , which agrees with twice the cavity mode frequency $2\omega_c$ to within 3%. This frequency corresponds to a timescale of 6 fs, matching the timescale of the fast oscillations observed in the dynamics of $q^2(t)$ and $\mu_{n,x}^2(t)$. The splitting between the two peaks is 545 cm^{-1} , which agrees with Ω_R to within 4%. Although it is reassuring that Ω_R appears in the spectrum as a splitting between a pair of peaks, we would usually expect to see that pair of peaks centered around ω_c and not $2\omega_c$. Interestingly, there are no features in the power spectrum of $q^2(t)$ in the region of the cavity mode frequency ω_c . These observations will be analyzed in more detail in the Discussion.

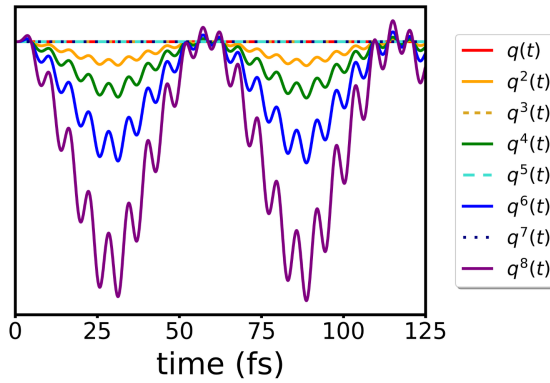


Figure 3. fq-RT-NEO dynamics of $q^n(t)$ for $n = 1, \dots, 8$. No units are given on the y -axis because these observables have different units.

The observation that the first-order quantities $q(t)$ and $\mu_{n,x}(t)$ are constant, while the quadratic quantities $q^2(t)$ and $\mu_{n,x}^2(t)$ oscillate, suggests the possibility of a more general trend, whereby the expectation values of odd powers of $\hat{q}_{k,x}$ and $\hat{\mu}_{n,x}$ are constant and the expectation values of even powers of these operators oscillate. To test this hypothesis, we plot $q^n(t) \equiv \text{Tr}[\mathbf{P}_F(t)\mathbf{q}_{k,x}^n] - \text{Tr}[\mathbf{P}_F(0)\mathbf{q}_{k,x}^n]$ for $n = 1 \dots 8$ in Figure 3 and find that this trend does hold. The expectation values of even powers oscillate, while the expectation values of odd powers of $\hat{q}_{k,\lambda}$ remain constant.

In Figure S1 in the Supporting Information, we show the corresponding plot for $\mu_{n,x}^n(t) \equiv \text{Tr}[\mathbf{P}_n(t)\boldsymbol{\mu}_{n,x}^n] - \text{Tr}[\mathbf{P}_n(0)\boldsymbol{\mu}_{n,x}^n]$ for $n = 1\dots 8$. The same trend for expectation values of even and odd operator powers holds for $\hat{\mu}_{n,x}$ as well. In Figure S2, we show the power spectrum of $\mu_{n,x}^2(t)$, which agrees qualitatively with the power spectrum of $q^2(t)$ shown in Figure 2. Figure S2a exhibits a peak at 565 cm^{-1} , perfectly matching the Ω_R peak in Figure 2a. Similar to Figure 2b, Figure S2b shows a pair of peaks separated by 555 cm^{-1} , which agrees with the Rabi splitting $\Omega_R = 565 \text{ cm}^{-1}$ to within 2%. This pair of peaks is centered at a frequency of 4918 cm^{-1} , which is redshifted from the center of the pair of peaks in the power spectrum of $q^2(t)$ by 519 cm^{-1} but still agrees with $2\omega_c = 5606 \text{ cm}^{-1}$ to within $\sim 12\%$. Finally, we note that by the argument given previously, all of these observables would be constant at the mfq-RT-NEO level of theory.

Our mfq-RT-NEO and fq-RT-NEO dynamics initialized with the molecule in its ground state and the cavity mode in a one-photon Fock state yielded several interesting results. In the mfq-RT-NEO simulation, coherent energy transfer between the molecule and the cavity mode was entirely suppressed, and polariton formation did not occur. Coherent energy transfer and significant light-matter entanglement did occur in the fq-RT-NEO simulation, but this interaction manifested only in the oscillations of even powers of the cavity mode coordinate and quantum nuclear dipole operators. Furthermore, the power spectra of these nonzero expectation values displayed spectral features that did not include the splitting of a bare molecular peak at the cavity mode frequency into two polariton peaks. Below, we will consider all of these results in more detail, aiming to facilitate our understanding through comparisons with analytically tractable quantum optics models.

V. DISCUSSION

In this section, we will employ quantum optical models to understand the key observations presented above in the fq-RT-NEO results: the lack of oscillations in $q(t)$ and $\mu_{n,x}(t)$, the spectral features of the power spectrum of $q^2(t)$ shown in Figure 2, and the trend in expectation values of $q^n(t)$ and $\mu_{n,x}^n(t)$ for even and odd powers of n shown in Figure 3 and Figure S1. First, we will use a quantum Rabi model Hamiltonian in a minimal basis to better understand the lack of oscillations in the dynamics of $q(t)$ and $\mu_{n,x}(t)$ and determine the criteria needed to recover the canonical feature of cavity-modified spectra, namely the splitting of a bare molecular transition into two polariton peaks. We will then consider the same model in a larger basis in order to explain the trend in expectation values of $q^n(t)$ and $\mu_{n,x}^n(t)$ for even and odd powers of n , as well as the spectral features and oscillation frequencies in Figures 2 and 3 and Figure S1.

Throughout this section, we will make extensive use of dressed-state kets in the joint light–matter Hilbert space denoted as $|FM\rangle$. We will adopt the convention that the quantum number F determines the number of photons populating the cavity mode, while M corresponds to the M^{th} eigenstate of the bare molecular subsystem.

A. Criteria for Oscillations of $q(t)$ and $\mu_{n,x}(t)$

We will first examine the requirements for oscillations of the expectation values of the cavity mode coordinate and molecular dipole moment operators. This understanding will clarify the criteria for the initial conditions required to observe the bare molecular peak split into two polariton peaks.

We consider a model quantum Rabi Hamiltonian of the form

$$\begin{aligned}
\hat{H} &= \hat{H}_F + \hat{H}_M + \varepsilon \hat{q} \hat{\mu} \\
&= \hat{H}_F + \hat{H}_M + \varepsilon q_0 (\hat{a}^\dagger + \hat{a}) \mu_0 (\hat{b}^\dagger + \hat{b}) \\
&= \omega \hat{a}^\dagger \hat{a} + \omega \hat{b}^\dagger \hat{b} + g (\hat{a}^\dagger \hat{b}^\dagger + \hat{a}^\dagger \hat{b} + \hat{a} \hat{b}^\dagger + \hat{a} \hat{b})
\end{aligned} \tag{17}$$

Here, we have taken $\hbar = 1$ in atomic units. As before, the subscript “F” denotes field, which refers to the cavity mode. We define \hat{a} (\hat{a}^\dagger) as the photon annihilation (creation) operator and \hat{b} (\hat{b}^\dagger) as the molecular excitation annihilation (creation) operator. In this notation, $\hat{q} = q_0 (\hat{a}^\dagger + \hat{a})$ is the mode coordinate operator, and $\hat{\mu} = \mu_0 (\hat{b}^\dagger + \hat{b})$ is the molecular dipole operator, where q_0 and μ_0 are constants that give their respective operators the appropriate dimensions. The light–matter coupling is given by $g = \varepsilon q_0 \mu_0$, where ε is a constant with appropriate dimensions, comparable to $\varepsilon_{k,\lambda}$ in Eq. 7, such that g has dimensions of energy. $\hat{H}_F = \omega \hat{a}^\dagger \hat{a}$ and $\hat{H}_M = \omega \hat{b}^\dagger \hat{b}$ are the bare cavity mode and molecular Hamiltonians, respectively. For simplicity, we assume the cavity mode to be in resonance with the molecular transition at energy ω in atomic units. Note that in this model, the vibrational mode is assumed to be harmonic. Finally, we point out that even though we take \hat{b} and \hat{b}^\dagger to be bosonic operators, our subsequent results would remain valid if these bosonic operators were replaced by fermionic creation and annihilation operators.

In this section, we consider this Hamiltonian in the basis of four dressed states: $|00\rangle$, $|11\rangle$, $|01\rangle$, and $|10\rangle$. In this basis, \mathbf{H} , the matrix representation of \hat{H} , factors into two 2×2 blocks:

$$\mathbf{H} = \begin{pmatrix} 0 & g \\ g & 2\omega \\ & \omega & g \\ & g & \omega \end{pmatrix} = \begin{pmatrix} \mathbf{H}_{\text{CR}} & \\ & \mathbf{H}_{\text{JC}} \end{pmatrix} \tag{18}$$

The lower right block, \mathbf{H}_{JC} , is the Hamiltonian of the Jaynes-Cummings model. It can be understood as the contribution of the terms $\hat{a}^\dagger \hat{b}$ and $\hat{a} \hat{b}^\dagger$ in Eq. 17. The upper left block, \mathbf{H}_{CR} , corresponds to the contribution of the double excitation and de-excitation counter-rotating terms $\hat{a}^\dagger \hat{b}^\dagger$ and $\hat{a} \hat{b}$ in Eq. 17. Application of the rotating wave approximation (RWA) to Eq. 17 would eliminate the counter-rotating terms and by extension the off-diagonal elements of \mathbf{H}_{CR} . We also note that for the four dressed states $|FM\rangle$, $F - M$ is even for states in the counterrotating block and is odd for states in the Jaynes-Cummings block. We will expand on this observation in more detail below.

We now diagonalize both \mathbf{H}_{JC} and \mathbf{H}_{CR} . The differences between the eigenenergies will determine the possible frequencies at which an observable evolving under the Hamiltonian \mathbf{H} could oscillate. The eigenenergies and eigenstates for \mathbf{H}_{JC} are

$$E_{\pm}^{JC} = \omega \pm g \quad (19)$$

$$|\psi_{\pm}^{JC}\rangle = \frac{1}{\sqrt{2}} (|01\rangle \pm |10\rangle) \quad (20)$$

The Rabi splitting is given by $\Omega_R = E_+^{JC} - E_-^{JC} = 2g$. The eigenenergies and eigenstates for \mathbf{H}_{CR} are

$$E_{\pm}^{CR} = \omega \pm \sqrt{\omega^2 + g^2} \quad (21)$$

$$|\psi_{\pm}^{CR}\rangle = -\frac{E_{\mp}^{CR}}{gN_{\pm}} |00\rangle + \frac{1}{N_{\pm}} |11\rangle \quad (22)$$

where we introduce the normalization constants $N_{\pm} \equiv \sqrt{1 + (E_{\mp}^{CR}/g)^2}$. Note that $|\psi_-^{CR}\rangle$ is the ground state in this basis. If we introduce transformation matrices

$$\mathbf{U}_{JC} = \begin{pmatrix} \frac{1}{\sqrt{2}} & \frac{1}{\sqrt{2}} \\ \frac{1}{\sqrt{2}} & -\frac{1}{\sqrt{2}} \end{pmatrix} \quad (23)$$

$$\mathbf{U}_{CR} = \begin{pmatrix} -\frac{E_-^{CR}}{gN_+} & -\frac{E_+^{CR}}{gN_-} \\ \frac{1}{N_+} & \frac{1}{N_-} \end{pmatrix} \quad (24)$$

then we can transform any matrix from the original basis of four dressed states to the eigenbasis of \mathbf{H} , $|\psi_{\pm}^{\text{CR}}\rangle$ and $|\psi_{\pm}^{\text{JC}}\rangle$ (hereafter denoted the “energy eigenbasis”), using the total transformation matrix given by the direct sum

$$\mathbf{U}_T = \mathbf{U}_{\text{CR}} \oplus \mathbf{U}_{\text{JC}} = \begin{pmatrix} \mathbf{U}_{\text{CR}} & \\ & \mathbf{U}_{\text{JC}} \end{pmatrix} \quad (25)$$

We now transform the matrices \mathbf{q} and $\boldsymbol{\mu}$, the matrix representations of the operators \hat{q} and $\hat{\mu}$, from the dressed-state basis to the energy eigenbasis using \mathbf{U}_T . In the dressed-state basis, these matrices are given by

$$\mathbf{q} = q_0 \begin{pmatrix} & 1 \\ & & 1 \\ & & & 1 \\ 1 & & & \end{pmatrix} = q_0(\boldsymbol{\sigma}_x \otimes \boldsymbol{\sigma}_x) \quad (26)$$

$$\boldsymbol{\mu} = \mu_0 \begin{pmatrix} & 1 \\ & & 1 \\ 1 & & & \\ & 1 & & \end{pmatrix} = \mu_0(\boldsymbol{\sigma}_x \otimes \mathbf{I}_2) \quad (27)$$

where $\boldsymbol{\sigma}_x$ is the Pauli x -matrix and \mathbf{I}_2 is the 2×2 identity matrix. Transforming to the energy eigenbasis, we obtain

$$\mathbf{q} \rightarrow \mathbf{U}_T^\dagger \mathbf{q} \mathbf{U}_T = q_0 \begin{pmatrix} & \mathbf{U}_{\text{CR}}^\dagger \boldsymbol{\sigma}_x \mathbf{U}_{\text{JC}} \\ \mathbf{U}_{\text{JC}}^\dagger \boldsymbol{\sigma}_x \mathbf{U}_{\text{CR}} & \end{pmatrix} \quad (28)$$

$$\boldsymbol{\mu} \rightarrow \mathbf{U}_T^\dagger \boldsymbol{\mu} \mathbf{U}_T = \mu_0 \begin{pmatrix} & \mathbf{U}_{\text{CR}}^\dagger \mathbf{U}_{\text{JC}} \\ \mathbf{U}_{\text{JC}}^\dagger \mathbf{U}_{\text{CR}} & \end{pmatrix} \quad (29)$$

We can immediately see from the block diagonal structures of Eqs. 28 and 29 why there are no oscillations of $q(t)$ and $\mu(t)$ in our fq-RT-NEO simulations when

the mode is initialized in a single-photon Fock state and the molecular system is initialized in its ground state, even though neither $\hat{\mu}$ nor \hat{q} commute with \hat{H} . In the model treatment here, the only nonzero matrix elements of \mathbf{q} and $\boldsymbol{\mu}$ are between the Jaynes-Cummings energy eigenstates $|\psi_{\pm}^{\text{JC}}\rangle$ and the counterrotating energy eigenstates $|\psi_{\pm}^{\text{CR}}\rangle$. Any state $|\Psi(t)\rangle$ of the joint light-matter system can be written as a linear combination of these four states:

$$|\Psi(t)\rangle = c_+^{\text{JC}} \exp(-iE_+^{\text{JC}}t) |\psi_+^{\text{JC}}\rangle + c_-^{\text{JC}} \exp(-iE_-^{\text{JC}}t) |\psi_-^{\text{JC}}\rangle + c_+^{\text{CR}} \exp(-iE_+^{\text{CR}}t) |\psi_+^{\text{CR}}\rangle + c_-^{\text{CR}} \exp(-iE_-^{\text{CR}}t) |\psi_-^{\text{CR}}\rangle \quad (30)$$

From Eq. 30, we can see that any time-dependent expectation value $A(t) = \langle \Psi(t) | \hat{A} | \Psi(t) \rangle$ of an operator \hat{A} will be a sum of terms of the form $c_i c_j^* \exp(-i(E_i - E_j)t) \langle j | \hat{A} | i \rangle$, where $\langle j |$ and $|i\rangle$ are energy eigenstates. These terms will oscillate with a frequency $(E_i - E_j)$, the difference in energy between $|i\rangle$ and $|j\rangle$, assuming that c_i and c_j , the coefficients of $|i\rangle$ and $|j\rangle$ at $t = 0$, as well as $\langle j | \hat{A} | i \rangle$, are all nonzero. Based on this analysis and the structure of the matrices \mathbf{q} and $\boldsymbol{\mu}$ given in Eqs. 28 and 29, we conclude that we will only observe oscillations in $q(t)$ and $\mu(t)$ if the initial state of the system can be written as a superposition of Jaynes-Cummings and counterrotating energy eigenstates with nonzero contributions from both types of eigenstates. The model initial condition corresponding to the initial condition of the fq-RT-NEO calculation in this work is the dressed state $|10\rangle = \frac{1}{\sqrt{2}} (|\psi_+^{\text{JC}}\rangle - |\psi_-^{\text{JC}}\rangle)$. This state is exclusively a superposition of Jaynes-Cummings eigenstates, and thus we do not observe any oscillations in $q(t)$ and $\mu_{n,x}(t)$. The oscillations of expectation values of higher powers of the operators \hat{q} and $\hat{\mu}$, denoted $q^n(t)$ and $\mu^n(t)$ with $n > 1$, will be considered in the next section.

If the initial state of the joint light-matter system can be written as a superposition of Jaynes-Cummings and counterrotating energy eigenstates with nonzero contributions from both types, then we will observe oscillations in $q(t)$ and $\mu(t)$. As

pointed out above, the frequencies of these oscillations will be given by the energy differences between the Jaynes-Cummings and counterrotating energy eigenstates. We will restrict our attention to positive energy differences without loss of generality. We first consider the energy differences between the Jaynes-Cummings polariton states and the ground state

$$E_{\pm}^{\text{JC}} - E_{-}^{\text{CR}} = \sqrt{\omega^2 + g^2} \pm g \quad (31)$$

Assuming that $\omega \gg g$, we can expand this difference in powers of the small quantity $g/\omega \ll 1$ to obtain a simple expression for the location of the peaks in the power spectra of $q(t)$ and $\mu(t)$:

$$\begin{aligned} E_{\pm}^{\text{JC}} - E_{-}^{\text{CR}} &= \sqrt{\omega^2 + g^2} \pm g \\ &= \omega \sqrt{1 + \left(\frac{g}{\omega}\right)^2} \pm g \\ &= \omega \left(1 + \frac{1}{2} \left(\frac{g}{\omega}\right)^2 + \dots\right) \pm g \\ &= \omega \pm g + O((g/\omega)^2) \end{aligned} \quad (32)$$

We therefore find that if our model system is initialized in a superposition of Jaynes-Cummings and counterrotating energy eigenstates with nonzero contributions from both types, then the power spectra of $q(t)$ and $\mu(t)$ exhibit a pair of peaks split by the Rabi splitting $\Omega_R = 2g$, with the center of the peaks at the bare molecular transition energy ω . Higher-order corrections to these energies are proportional to terms that are second order in the small quantity (g/ω) . This same analysis can also be carried out for the other set of positive energy differences, $E_{+}^{\text{CR}} - E_{\pm}^{\text{JC}}$, with identical results.

Finally, we observe that within the framework of this model and basis set, initializing the total light-matter system in a superposition of Jaynes-Cummings and counterrotating eigenstates is equivalent to the case in which at least one of the light

or matter subsystems is in a superposition of its ground and excited states. In Ref. 61, we initialized the joint light–matter system for our fq-RT-NEO calculations as a separable product of a coherent state of the cavity mode and the molecular ground state. A coherent state is by definition a superposition of ground and excited states, so we expect to see a bare molecular transition peak split into two peaks separated by the Rabi splitting. Since a classical mode shows qualitatively similar behavior to a quantum mode prepared in a coherent state with the analogous initial coordinate and momentum values, we expect this same phenomenon to appear with a classical mode as well. This behavior was observed for both the classical and quantum cavity mode RT-NEO simulations in Ref. 61.

B. Oscillations of $q^n(t)$ and $\mu^n(t)$ for even n

The power rule for even and odd expectation values of $q^n(t)$ and $\mu^n(t)$ shown by the data in Figure 3 and Figure S1 can be understood by considering the quantum Rabi Hamiltonian given in Eq. 17, but *in a larger basis set*. To understand the need to use a larger basis set, we look at powers of the matrix representations \mathbf{q} and $\boldsymbol{\mu}$ in the four-state energy eigenbasis that we have employed thus far. Using Eqs. 28 and 29, as well as the fact that $\boldsymbol{\sigma}_x^2 = \mathbf{I}_2$, we obtain

$$\mathbf{q}^n = \begin{cases} q_0^n \begin{pmatrix} & \mathbf{U}_{\text{CR}}^\dagger \boldsymbol{\sigma}_x \mathbf{U}_{\text{JC}} \\ \mathbf{U}_{\text{JC}}^\dagger \boldsymbol{\sigma}_x \mathbf{U}_{\text{CR}} & \end{pmatrix} & (n \text{ odd}) \\ q_0^n \begin{pmatrix} \mathbf{I}_2 & \\ & \mathbf{I}_2 \end{pmatrix} & (n \text{ even}) \end{cases} \quad (33)$$

$$\boldsymbol{\mu}^n = \begin{cases} \mu_0^n \begin{pmatrix} & \mathbf{U}_{\text{CR}}^\dagger \mathbf{U}_{\text{JC}} \\ \mathbf{U}_{\text{JC}}^\dagger \mathbf{U}_{\text{CR}} & \end{pmatrix} & (n \text{ odd}) \\ \mu_0^n \begin{pmatrix} \mathbf{I}_2 & \\ & \mathbf{I}_2 \end{pmatrix} & (n \text{ even}) \end{cases} \quad (34)$$

This result presents what appears to be a contradiction. Eqs. 33 and 34 seem to state that for even n , $[\hat{H}, \hat{\mu}^n] = [\hat{H}, \hat{q}^n] = 0$, as their matrix representations can be diagonalized in the same basis set. This would imply that the expectation values of the operators are constants of motion for even powers n , regardless of whether the initial condition for the cavity mode is a Fock state, coherent state, or some other state. This result disagrees with Figure 3 and Figure S1, which shows oscillations of the expectation values of \hat{q}^n and $\hat{\mu}^n$ for even n when the cavity mode initial condition is a Fock state. In addition to disagreeing with the results of our simulations, the aforementioned commutation relation can also be proven false algebraically using the definitions of these operators given in Eq. 17 and the subsequent text.

The resolution of this contradiction comes when we realize that $[\hat{H}, \hat{\mu}^n] = [\hat{H}, \hat{q}^n] = 0$ for even n only if we are treating both the light and matter subsystems as two-level systems, i.e., the relation is only true within the specific subspace of the joint light–matter Hilbert space considered thus far. To see how this comes about, we consider the commutator $[\hat{H}, \hat{\mu}^2]$, which we can evaluate:

$$\begin{aligned} [\hat{H}, \hat{\mu}^2] &= [\omega \hat{b}^\dagger \hat{b}, \mu_0^2 (\hat{b}^\dagger \hat{b} + \hat{b} \hat{b}^\dagger + \hat{b} \hat{b}^\dagger + \hat{b}^\dagger \hat{b}^\dagger)] \\ &= [\omega \hat{b}^\dagger \hat{b}, \mu_0^2 (\hat{b}^\dagger \hat{b} + (1 + \hat{b}^\dagger \hat{b}) + \hat{b} \hat{b}^\dagger + \hat{b}^\dagger \hat{b}^\dagger)] \\ &= [\omega \hat{b}^\dagger \hat{b}, \mu_0^2 (\hat{b} \hat{b}^\dagger + \hat{b}^\dagger \hat{b}^\dagger)] \\ &= 2\omega \mu_0^2 (\hat{b}^\dagger \hat{b}^\dagger - \hat{b} \hat{b}) \end{aligned} \quad (35)$$

At the second equality, we have used the commutation relation for bosonic operators $[\hat{b}, \hat{b}^\dagger] = 1$. Eq. 35 is clearly nonzero in general, but if the molecular subsystem is taken to be a two-level system, then the double excitation (deexcitation) operator $\hat{b}^\dagger \hat{b}^\dagger$ ($\hat{b} \hat{b}$) returns zero if it acts on any state ket. These operators can therefore be taken to be zero, and we then obtain $[\hat{H}, \hat{\mu}^2] = 0$. The same result can be shown to hold for $[\hat{H}, \hat{q}^2]$ simply by taking the cavity mode to be a two-level system and making the replacement $\hat{b} \rightarrow \hat{a}$, recognizing that \hat{a} satisfies $[\hat{a}, \hat{a}^\dagger] = 1$. This result also holds if the bosonic operators \hat{b} and \hat{b}^\dagger describing the molecular system are replaced by fermionic operators; the proof is given in Section 3 of the Supplementary Material.

The above result makes it clear that we need to determine the structure of \mathbf{q}^n and $\boldsymbol{\mu}^n$ in a larger energy eigenbasis, i.e., we must increase the dimensionality of the subsystems. To expand the eigenbasis, we will first consider the structures of the matrices \mathbf{H} , \mathbf{q} , and $\boldsymbol{\mu}$ in an extended dressed-state basis. We will then convert \mathbf{q} and $\boldsymbol{\mu}$ into the corresponding energy eigenbasis that diagonalizes \mathbf{H} . Finally, we will take powers of these matrices to prove the even-odd power rule in our model.

We first prove that the block-diagonal structure of \mathbf{H} as a direct sum of counterrotating and Jaynes-Cummings blocks, as shown in Eq. 18, is a general result that holds for a dressed-state basis of any size. We start by recognizing that all states in the counterrotating block must in some sense be “connected” to the state $|00\rangle$ through the operation of the light-matter coupling operator \hat{V} . For notational simplicity, we will use the subscript D in lieu of specifying two quantum numbers for the field and molecular degrees of freedom. Formally, two dressed states $|i_D\rangle$ and $|f_D\rangle$ are connected if $|f_D\rangle$ is a member of a set $\{|j_D\rangle\}$ such that for some positive integer $m \geq 1$, we can write

$$\hat{V}^m |i_D\rangle = \sum_j c_j |j_D\rangle \quad (36)$$

where all $|c_j| > 0$. In Eq. 36, \hat{V} is given by

$$\hat{V} = g(\hat{a}^\dagger + \hat{a})(\hat{b}^\dagger + \hat{b}) = g(\hat{a}^\dagger \hat{b}^\dagger + \hat{a}^\dagger \hat{b} + \hat{a} \hat{b}^\dagger + \hat{a} \hat{b}) \quad (37)$$

Eq. 37 defines four operations: double excitation ($\hat{a}^\dagger \hat{b}^\dagger$), excitation-deexcitation ($\hat{a}^\dagger \hat{b}$), deexcitation-excitation ($\hat{a} \hat{b}^\dagger$), and double deexcitation ($\hat{a} \hat{b}$). These operators, respectively, increase both quantum numbers F and M by 1; increase F and decrease M , both by 1; decrease F and increase M , both by 1; and decrease both quantum numbers F and M by 1. Any state $|FM\rangle$ is in the counterrotating block if it can be connected to the state $|00\rangle$ through any combination of these four operations. Likewise, we can also say that a state $|FM\rangle$ is in the Jaynes-Cummings block if it can be connected to the state $|01\rangle$ through any combination of these four operations. This approach implies a tree structure of the dressed states in each of the counterrotating and Jaynes-Cummings blocks, as shown in Figure 4.

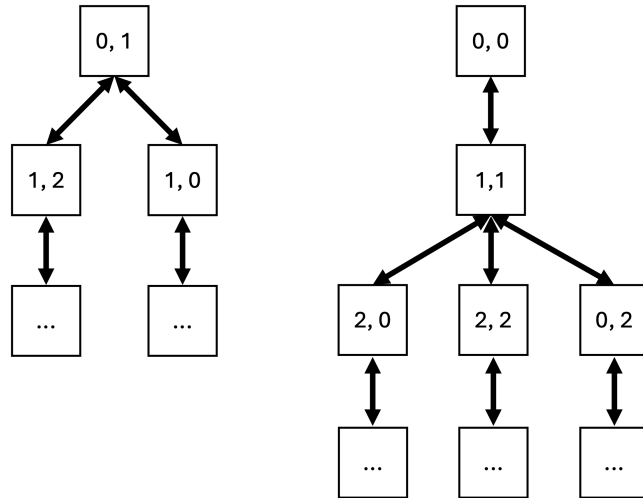


Figure 4. Structure of the trees corresponding to the Jaynes-Cummings (left) and counter-rotating (right) blocks of \mathbf{H} . Each tree is shown up to the first layer with more than one node.

To prove the desired result, we must prove (a) that any state $|FM\rangle$ can be assigned to one of these two trees, and (b) that these two trees can never be connected by the set of operations given above. To prove (a), we note that for any dressed state $|FM\rangle$, repeated application of the excitation-deexcitation operator (if $F < M$) or the deexcitation-excitation operator (if $F > M$) will eventually connect to a state $|GH\rangle$ where $G = H$ or $G = H \pm 1$. Which outcome occurs will depend on whether $F - M$ is even or odd. If $F - M$ is even, then we will eventually obtain $G = H$, putting us at a state on the trunk of the counterrotating tree in Figure 4. Repeated application of the double deexcitation operator will then eventually yield $|00\rangle$. If $F - M$ is odd, then we will eventually obtain $G = H \pm 1$. Repeated application of the double deexcitation operator will then lead to either $|01\rangle$ or $|10\rangle$; $|10\rangle$ can be connected to $|01\rangle$ by applying the deexcitation-excitation operation. Therefore, any state $|FM\rangle$ belongs to one of the two trees in Figure 4. Furthermore, it follows from this analysis that the two trees can never be connected. The states $|FM\rangle$ in the Jaynes-Cummings tree satisfy the criterion that $F - M$ is odd, whereas the states $|FM\rangle$ in the counterrotating tree satisfy the criterion that $F - M$ is even. None of the four operations given above can change the parity of the difference $F - M$, i.e., they cannot connect a state where $F - M$ is even to one where it is odd and vice versa. Hence, the two trees cannot be connected, and the proof is complete.

We have established that the Hamiltonian can be written in the form

$$\mathbf{H} = \begin{pmatrix} \mathbf{H}_{\text{CR}} & \\ & \mathbf{H}_{\text{JC}} \end{pmatrix} \quad (38)$$

in any basis of dressed states $|FM\rangle$. This implies that the matrix \mathbf{U} that diagonalizes \mathbf{H} can be written as in Eq. 25:

$$\mathbf{U} = \begin{pmatrix} \mathbf{U}_{\text{CR}} & \\ & \mathbf{U}_{\text{JC}} \end{pmatrix} \quad (39)$$

We can also show that the matrices \mathbf{q} and $\boldsymbol{\mu}$, when written in such a general dressed-state basis, have the form

$$\begin{pmatrix} & \mathbf{M}^\dagger \\ \mathbf{M} & \end{pmatrix} \quad (40)$$

To prove this, we note that the operators $\hat{q} = q_0(\hat{a} + \hat{a}^\dagger)$ and $\hat{\mu} = \mu_0(\hat{b} + \hat{b}^\dagger)$ can only have matrix elements between states $|FM\rangle$ with opposite parity of the difference $F - M$, i.e., a pair of states where $F - M$ is odd for one state and even for the other. This is because a single action of \hat{a} or \hat{b} , or their Hermitian conjugates \hat{a}^\dagger and \hat{b}^\dagger , will change either F or M by 1, and thereby switch the parity of the difference $F - M$. The Jaynes-Cummings and counterrotating blocks all have states of the same difference parity, so any nonzero elements of \mathbf{q} and $\boldsymbol{\mu}$ must be in the off-diagonal blocks. The additional requirement that these matrices must be Hermitian implies the structure shown in Eq. 40.

Using the transformation matrix \mathbf{U} to transform a matrix of the form given in Eq. 40 into the energy eigenbasis does not change its off-diagonal block structure:

$$\begin{pmatrix} & \mathbf{M}^\dagger \\ \mathbf{M} & \end{pmatrix} \rightarrow \begin{pmatrix} & \mathbf{M}'^\dagger \\ \mathbf{M}' & \end{pmatrix} = \begin{pmatrix} & \mathbf{U}_{\text{CR}}^\dagger \mathbf{M}^\dagger \mathbf{U}_{\text{JC}} \\ \mathbf{U}_{\text{JC}}^\dagger \mathbf{M} \mathbf{U}_{\text{CR}} & \end{pmatrix} \quad (41)$$

In the case of two two-level systems, as treated above in Eqs. 28 and 29, $\mathbf{M}' = \mathbf{U}_{\text{JC}}^\dagger \boldsymbol{\sigma}_x \mathbf{U}_{\text{CR}}$ and $\mathbf{U}_{\text{JC}}^\dagger \mathbf{U}_{\text{CR}}$ for \mathbf{q} and $\boldsymbol{\mu}$, respectively. In this minimal basis set, \mathbf{M}' is unitary for both operators; as discussed above, this is a consequence of that choice of basis set and is not true in general.

If we take powers of Eq. 41, we find that we alternate between an off-diagonal block structure for odd powers of n and a block diagonal structure for even powers of n . Since $[\hat{H}, \hat{q}^n] \neq 0$ and $[\hat{H}, \hat{\mu}^n] \neq 0$, the blocks will in general not be diagonal, with the exception, as discussed above, of the minimal basis set where both the molecule and cavity mode subsystems are treated as two-level systems. Thus, for even powers

n , there will be nonzero matrix elements between different Jaynes-Cummings energy eigenstates and between different counterrotating energy eigenstates. We will therefore observe oscillations of $q^n(t)$ and $\mu^n(t)$ for even n when the dynamics is initialized in the superposition of Jaynes-Cummings eigenstates $|10\rangle = \frac{1}{\sqrt{2}} (|\psi_+^{\text{JC}}\rangle - |\psi_-^{\text{JC}}\rangle)$. For odd powers n , however, we will not observe oscillations because of the off-diagonal block structure of Eq. 41. This result is true for any situation where the two subsystems are each treated as an m -level subsystem, where $m > 2$.

The frequencies of oscillation of $q^n(t)$ and $\mu^n(t)$ will be determined by diagonalization of \mathbf{H} in a given basis. In the next section, we will diagonalize the Hamiltonian given in Eq. 17 in the smallest basis required to observe oscillations of $q^2(t)$, and we will compare the frequencies of oscillation predicted by the model with the frequencies obtained from the power spectrum of $q^2(t)$ in Figure 2.

C. Origin of fq-RT-NEO Spectral Features

Our previous analysis will now help us understand the origins of the spectral features in the power spectrum of $q^2(t)$ shown in Figure 2 above. To reduce the dimensionality of our model to a minimum while still capturing all major qualitative features, we will treat the molecule as a two-level system and the cavity mode as a three-level system. As established in the previous section, treating the cavity mode as a three-level system is the minimum basis set size required to obtain nonzero matrix elements of \hat{q}^2 between Jaynes-Cummings energy eigenstates, and therefore to observe oscillations of $q^2(t)$ when the joint light-matter system is initialized in the dressed state $|10\rangle = \frac{1}{\sqrt{2}} (|\psi_+^{\text{JC}}\rangle - |\psi_-^{\text{JC}}\rangle)$. We will therefore represent the Hamiltonian in Eq. 17 in the basis of six dressed states: $|00\rangle, |11\rangle, |20\rangle, |01\rangle, |10\rangle$, and $|21\rangle$. As proven in the previous section, the matrix representation of Eq. 17 in this basis is block diagonal and factors into Jaynes-Cummings and counterrotating blocks,

analogous to Eq. 18.

Within this matrix, we will restrict our attention to the Jaynes-Cummings block, which contains the dressed state $|10\rangle$ corresponding to the fq-RT-NEO initial condition. This block is the matrix representation of the Hamiltonian in Eq. 18 in the basis $|01\rangle, |10\rangle$, and $|21\rangle$, and is given by

$$\mathbf{H}_{\text{JC}} = \begin{pmatrix} \omega & g & 0 \\ g & \omega & \sqrt{2}g \\ 0 & \sqrt{2}g & 3\omega \end{pmatrix} \quad (42)$$

To determine the possible frequencies of oscillation of $q^2(t)$, we need to determine the differences between the energy eigenvalues of \mathbf{H}_{JC} . We will proceed via perturbation theory by taking the light-matter coupling matrix elements g to be the perturbation and the three dressed states to be the unperturbed states. The two-fold degeneracy in the upper-left block spanned by $|01\rangle$ and $|10\rangle$ means that we first need to diagonalize the perturbation in that subspace, thereby providing the first-order perturbative correction. We can achieve this by transforming with the matrix

$$\mathbf{U}_{\text{JC}} = \frac{1}{\sqrt{2}} \begin{pmatrix} 1 & 1 & 0 \\ 1 & -1 & 0 \\ 0 & 0 & \sqrt{2} \end{pmatrix} \quad (43)$$

This matrix will transform \mathbf{H}_{JC} into the zeroth-order basis $|\text{UP}\rangle = \frac{1}{\sqrt{2}}(|01\rangle + |10\rangle)$, $|\text{LP}\rangle = \frac{1}{\sqrt{2}}(|01\rangle - |10\rangle)$, and $|21\rangle$. $|\text{LP}\rangle$ and $|\text{UP}\rangle$ are the lower and upper polariton states that would be obtained by solving the Jaynes-Cummings model for two coupled two-level systems. Transformation of \mathbf{H}_{JC} yields

$$\mathbf{H}_{\text{JC}} \rightarrow \mathbf{U}_{\text{JC}}^\dagger \mathbf{H}_{\text{JC}} \mathbf{U}_{\text{JC}} = \begin{pmatrix} \omega + g & g & 0 \\ g & \omega - g & g \\ 0 & g & 3\omega \end{pmatrix} \quad (44)$$

Corrected to second order, the energies of the states $|LP\rangle$, $|UP\rangle$, and $|21\rangle$ are

$$E_{LP} = \omega - g - \frac{g^2}{2\omega + g} \quad (45)$$

$$E_{UP} = \omega + g - \frac{g^2}{2\omega - g} \quad (46)$$

$$E_{21} = 3\omega + \frac{g^2}{2\omega + g} + \frac{g^2}{2\omega - g} \quad (47)$$

Note that the last two terms in Eq. 47 are approximately equal for $g \ll \omega$. We will thus refer to them both as $A = \frac{g^2}{2\omega+g} \approx \frac{g^2}{2\omega-g}$ in Eqs. 45 - 47. We can now compute the differences between the energy eigenvalues:

$$\begin{aligned} E_{UP} - E_{LP} &= 2g = \Omega_R \\ E_{21} - E_{UP} &= 2\omega - g + 3A \\ E_{21} - E_{LP} &= 2\omega + g + 3A \end{aligned} \quad (48)$$

Eq. 48 indicates that within this three-state model, if we assume that \hat{q}^2 has nonzero matrix elements between all three eigenstates of \mathbf{H}_{JC} , which will be checked below for this model, then the power spectrum of $q^2(t)$ should show a peak at $\Omega_R = 2g$ as well as a pair of peaks centered at approximately 2ω with a splitting of $\Omega_R = 2g$. No features appear in the region of ω .

These findings are in excellent qualitative agreement with the data shown in Figure 2. Our sense of the quality of this agreement can be further enhanced by developing a comparison of the relative sizes of 2ω and A . To obtain a rough sense of the magnitude of A relative to ω and g , we can expand it in powers of the small quantity $g/2\omega$ to find that $A \approx g \left(\frac{g}{2\omega}\right)$. This result suggests that A is likely multiple orders of magnitude smaller than 2ω , further justifying our interpretation that the pair of peaks in our three-level model will be centered very nearly at 2ω . If we compare our model to the fq-RT-NEO results in Figure 2a, we can identify $g = \Omega_R/2 \approx 283 \text{ cm}^{-1}$.

Given that $\omega = 2803 \text{ cm}^{-1}$, we then find $A \approx g(g/2\omega) = 14 \text{ cm}^{-1}$, which is more than two orders of magnitude smaller than $2\omega = 5606 \text{ cm}^{-1}$. We acknowledge that comparison of our model results to the fq-RT-NEO results at an energy scale as small as 14 cm^{-1} is unlikely to succeed due to our model's simplicity. The approximations underlying our model include its low dimensionality, neglect of permanent dipole moments and transition dipoles between non-consecutive energy eigenstates, and absence of anharmonicity in the proton vibrational mode that would be captured by RT-NEO,⁶⁴ among other limitations. However, we are encouraged by the general qualitative agreement between this model and our fq-RT-NEO results.

As mentioned above, we will end by checking that there are nonzero matrix elements between all of the eigenstates of \mathbf{H}_{JC} . We can write the matrix \mathbf{q}^2 in the dressed-state basis and then transform it using \mathbf{U}_{JC} . In the dressed-state basis, we have

$$\mathbf{q}^2 = q_0^2 \begin{pmatrix} 1 & \sqrt{2} \\ 3 & \sqrt{2} \\ \sqrt{2} & 2 \end{pmatrix} \quad (49)$$

Transformation with \mathbf{U}_{JC} then yields

$$\mathbf{q}^2 \rightarrow \mathbf{U}_{\text{JC}}^\dagger \mathbf{q}^2 \mathbf{U}_{\text{JC}} = q_0^2 \begin{pmatrix} 2 & -1 & 1 \\ -1 & 2 & 1 \\ 1 & 1 & 2 \end{pmatrix} \quad (50)$$

This matrix gives \mathbf{q}^2 in the zeroth-order basis defined above. To obtain matrix elements of \mathbf{q}^2 in a more exact energy eigenbasis, we could perturbatively correct the zeroth-order states and further transform \mathbf{q}^2 into this corrected basis. However, as shown in the discussion above, reasonable qualitative agreement between this three-level model and the fq-RT-NEO results can be obtained, even if perturbative corrections to the zeroth-order states are neglected. Therefore, Eq. 50 is considered

to be a good approximation to the matrix representation of \hat{q}^2 in the exact eigenbasis of \mathbf{H}_{JC} . Given that there are nonzero matrix elements between all three unique pairs of eigenstates of \mathbf{H}_{JC} , we can confirm that a power spectrum of our model treatment of $q^2(t)$ will have three peaks, one around $2g = \Omega_R$, and the other two centered around 2ω and split by Ω_R . No features will be observed in the region around ω . This behavior is in excellent agreement with the fq-RT-NEO results shown in Figure 2.

Finally, we point out the good qualitative agreement between the spectral features predicted by Eq. 48 and the features in the power spectrum of $\mu_{n,x}^2(t)$ shown in Figure S2 of the Supporting Information. This agreement is intuitively reasonable if we assume that the dipole moment matrix $\boldsymbol{\mu}$ is similar in structure to the matrix \mathbf{q} , which we have analyzed in this section. The redshift of the center of the pair of peaks relative to 2ω , which also occurs to a lesser degree in the power spectrum of $q^2(t)$ shown in Figure 2, likely reflects phenomena that cannot be captured by the simple three-level model employed here.

VI. CONCLUSIONS

In this work, we used our previously developed mfq-RT-NEO and fq-RT-NEO methods to search for unique behavior in real-time polaritonic dynamics obtained when the cavity mode is initialized in a Fock state and an HCN molecule is initialized in its ground state. Such an initial condition corresponds to the picture of coherent energy transfer in polaritonic systems obtained from model treatments. Under this initial condition, the mfq-RT-NEO dynamics show no oscillation of the expectation values of the cavity mode coordinate and molecular quantum nuclear dipole moment operators, suggesting that coherent energy exchange and the associated polariton formation between the molecule and cavity mode do not occur at this level of theory.

Our analysis shows that under these initial conditions, the mfq-RT-NEO method predicts no time evolution of the molecular and cavity mode subsystems. Such behavior illustrates the limitations of the mean-field quantum method, as well as classical cavity mode approaches, which do not allow an initial cavity mode Fock state to produce polaritonic states.

Under the same initial conditions, fq-RT-NEO dynamics also show no oscillations of the expectation values of the cavity mode coordinate and molecular quantum nuclear dipole moment operators. In this full-quantum treatment, however, other evidence of polariton formation is observed. The von Neumann entropy $S(t)$, which is a measure of the quantum entanglement between the molecule and the cavity mode, oscillates significantly, reaching a maximum observed value of nearly 50% of the theoretical maximum value that could be observed with the simulation parameters used. Such light-matter entanglement implies polariton formation caused by coherent energy exchange between the molecule and the cavity mode. Interestingly, the expectation values of even powers of the coordinate and dipole moment operators oscillate, implicating polariton formation, whereas the expectation values of odd powers of these operators remain constant throughout the dynamics. The power spectrum of the expectation value of the square of the cavity mode coordinate operator reveals three major peaks. A single peak appears in the lower-energy region of the spectrum and can be interpreted as the Rabi splitting Ω_R , while two other peaks are centered at approximately twice the cavity mode frequency and split by Ω_R . All these observations can be rationalized by comparison to the quantum Rabi model. These models also help understand what conditions are required to observe the canonical feature of polariton formation, namely, a bare molecular transition peak splitting into two polariton peaks separated by a Rabi splitting.

These findings suggest that quantum electrodynamics may demonstrate new phenomena that are inaccessible to classical electrodynamics. This analysis also high-

lights the limitations of the traditional Jaynes-Cummings picture of polariton formation, where both subsystems are treated as two-level systems within the rotating wave approximation. Moving beyond the rotating wave approximation and considering a larger basis set for at least one of the subsystems can be important for even a qualitative understanding of molecular polariton dynamics. Thus, these findings justify the development and use of first-principles dynamics methods in the investigation of polariton chemistry. Future work will build upon these insights in an effort to achieve an atomistic-level understanding of the chemistry of molecular polaritonic systems.

SUPPLEMENTARY MATERIAL

The supplementary material contains a representative Q-Chem input file and molecular geometry for the reported results, fq-RT-NEO results for $\mu_{n,x}^n(t)$ for $n = 1, \dots, 8$, the power spectrum of $\mu_{n,x}^2(t)$, and the proof of the commutator algebra corresponding to Eq. 35 for fermionic operators.

ACKNOWLEDGMENTS

This material is based upon work supported by the Air Force Office of Scientific Research under AFOSR Award No. FA9550-24-1-0347. We thank Marissa Weichman, Scott Garner, Jonathan Fetherolf, Tim Duong, Arghadip Koner, Joel-Yuen Zhou, Chiara Aieta, Eno Paenurk, and Joseph Dickinson for helpful discussions.

DATA AVAILABILITY STATEMENT

The data that support the findings of this study will be openly available in Zenodo.

Conflict of Interest

The authors have no conflicts to disclose.

REFERENCES

¹A. Mandal, M. A. Taylor, B. M. Weight, E. R. Koessler, X. Li, and P. Huo, “Theoretical Advances in Polariton Chemistry and Molecular Cavity Quantum Electrodynamics,” *Chem. Rev.* **123**, 9786–9879 (2023).

²W. Xiong, “Molecular Vibrational Polariton Dynamics: What Can Polaritons Do?” *Acc. Chem. Res.* **56**, 776–786 (2023).

³M. Pelton, S. D. Storm, and H. Leng, “Strong coupling of emitters to single plasmonic nanoparticles: Exciton-induced transparency and Rabi splitting,” *Nanoscale* **11**, 14540–14552 (2019).

⁴B. Xiang and W. Xiong, “Molecular Polaritons for Chemistry, Photonics and Quantum Technologies,” *Chem. Rev.* **124**, 2512–2552 (2024).

⁵T. E. Li, B. Cui, J. E. Subotnik, and A. Nitzan, “Molecular Polaritonics: Chemical Dynamics Under Strong Light–Matter Coupling,” *Annual Review of Physical Chemistry* **73**, 43–71 (2022).

⁶H. Deng, H. Haug, and Y. Yamamoto, “Exciton-polariton Bose-Einstein condensation,” *Rev. Mod. Phys.* **82**, 1489–1537 (2010).

⁷J. Keeling and S. Kéna-Cohen, “Bose–Einstein Condensation of Exciton-Polaritons in Organic Microcavities,” *Annu. Rev. Phys. Chem.* **71**, 435–459 (2020).

⁸J. P. Long and B. S. Simpkins, “Coherent Coupling between a Molecular Vibration and Fabry–Perot Optical Cavity to Give Hybridized States in the Strong Coupling Limit,” *ACS Photonics* **2**, 130–136 (2015).

⁹J. George, A. Shalabney, J. A. Hutchison, C. Genet, and T. W. Ebbesen, “Liquid-Phase Vibrational Strong Coupling,” *J. Phys. Chem. Lett.* **6**, 1027–1031 (2015).

¹⁰A. D. Wright, J. C. Nelson, and M. L. Weichman, “Rovibrational Polaritons in Gas-Phase Methane,” *J. Am. Chem. Soc.* **145**, 5982–5987 (2023).

¹¹X. Zhong, T. Chervy, L. Zhang, A. Thomas, J. George, C. Genet, J. A. Hutchison, and T. W. Ebbesen, “Energy Transfer between Spatially Separated Entangled Molecules,” *Angew. Chem. Int. Ed.* **56**, 9034–9038 (2017).

¹²B. Xiang, R. F. Ribeiro, M. Du, L. Chen, Z. Yang, J. Wang, J. Yuen-Zhou, and W. Xiong, “Intermolecular vibrational energy transfer enabled by microcavity strong light–matter coupling,” *Science* **368**, 665–667 (2020).

¹³F. J. Garcia-Vidal, C. Ciuti, and T. W. Ebbesen, “Manipulating matter by strong coupling to vacuum fields,” *Science* **373**, 178 (2021).

¹⁴K. Georgiou, R. Jayaprakash, A. Othonos, and D. G. Lidzey, “Ultralong-Range Polariton-Assisted Energy Transfer in Organic Microcavities,” *Angew. Chem. Int. Ed.* **60**, 16661–16667 (2021).

¹⁵C. Kertzscher, M. Mauch, J. Keck, and A. J. Meixner, “A tunable Fabry-Pérot microcavity enables systematic investigation of strong light-matter coupling and energy transfer at distances of several μm ,” in *2024 24th International Conference on Transparent Optical Networks (ICTON)* (IEEE, Bari, Italy, 2024) pp. 1–3.

¹⁶D. G. Lidzey, D. D. C. Bradley, M. S. Skolnick, T. Virgili, S. Walker, and D. M. Whittaker, “Strong exciton–photon coupling in an organic semiconductor microcavity,” *Nature* **395**, 53–55 (1998).

¹⁷J. Feist and F. J. Garcia-Vidal, “Extraordinary Exciton Conductance Induced by Strong Coupling,” *Phys. Rev. Lett.* **114**, 196402 (2015).

¹⁸J. Schachenmayer, C. Genes, E. Tignone, and G. Pupillo, “Cavity-Enhanced Transport of Excitons,” *Phys. Rev. Lett.* **114**, 196403 (2015).

¹⁹D. M. Coles, N. Somaschi, P. Michetti, C. Clark, P. G. Lagoudakis, P. G. Savvidis, and D. G. Lidzey, “Polariton-mediated energy transfer between organic dyes in a strongly coupled optical microcavity,” *Nat. Mater.* **13**, 712–719 (2014).

²⁰J. Kasprzak, M. Richard, S. Kundermann, A. Baas, P. Jeambrun, J. M. J. Keeling, F. M. Marchetti, M. H. Szymańska, R. André, J. L. Staehli, V. Savona, P. B. Littlewood, B. Deveaud, and L. S. Dang, “Bose–Einstein condensation of exciton polaritons,” *Nature* **443**, 409–414 (2006).

²¹W. Ahn, J. F. Triana, F. Recabal, F. Herrera, and B. S. Simpkins, “Modification of ground-state chemical reactivity via light–matter coherence in infrared cavities,” *Science* **380**, 1165–1168 (2023).

²²A. Thomas, A. Jayachandran, L. Lethuillier-Karl, R. M. A. Vergauwe, K. Nagarajan, E. Devaux, C. Genet, J. Moran, and T. W. Ebbesen, “Ground state chemistry under vibrational strong coupling: Dependence of thermodynamic parameters on the Rabi splitting energy,” *Nanophotonics* **9**, 249–255 (2020), publisher: De Gruyter.

²³J. Lather, P. Bhatt, A. Thomas, T. W. Ebbesen, and J. George, “Cavity Catalysis by Cooperative Vibrational Strong Coupling of Reactant and Solvent Molecules,” *Angew. Chem. Int. Ed.* **58**, 10635–10638 (2019).

²⁴A. Thomas, L. Lethuillier-Karl, K. Nagarajan, R. M. A. Vergauwe, J. George, T. Chervy, A. Shalabney, E. Devaux, C. Genet, J. Moran, and T. W. Ebbesen, “Tilting a ground-state reactivity landscape by vibrational strong coupling,” *Science* **363**, 615–619 (2019).

²⁵E. Jaynes and F. Cummings, “Comparison of quantum and semiclassical radiation theories with application to the beam maser,” *IEEE Proc.* **51**, 89–109 (1963).

²⁶M. Tavis and F. W. Cummings, “Exact Solution for an N-Molecule—Radiation-Field Hamiltonian,” *Phys. Rev.* **170**, 379–384 (1968).

²⁷M. Tavis and F. W. Cummings, “Approximate Solutions for an N-Molecule—Radiation-Field Hamiltonian,” *Phys. Rev.* **188**, 692–695 (1969).

²⁸C. Schäfer, M. Ruggenthaler, and A. Rubio, “*Ab initio* nonrelativistic quantum electrodynamics: Bridging quantum chemistry and quantum optics from weak to strong coupling,” *Phys. Rev. A* **98**, 043801 (2018).

²⁹A. E. DePrince, III, “Cavity-modulated ionization potentials and electron affinities from quantum electrodynamics coupled-cluster theory,” *J. Chem. Phys.* **154**, 094112 (2021).

³⁰J. D. Mallory and A. E. DePrince, “Reduced-density-matrix-based *Ab initio* cavity quantum electrodynamics,” *Phys. Rev. A* **106**, 053710 (2022).

³¹N. Vu, D. Mejia-Rodriguez, N. P. Bauman, A. Panyala, E. Mutlu, N. Govind, and J. J. I. Foley, “Cavity Quantum Electrodynamics Complete Active Space Configuration Interaction Theory,” *J. Chem. Theory Comput.* **20**, 1214–1227 (2024).

³²Y. El Moutaoukal, R. R. Riso, M. Castagnola, E. Ronca, and H. Koch, “Strong Coupling Møller–Plesset Perturbation Theory,” *J. Chem. Theory Comput.* **21**, 3981–3992 (2025).

³³M. Bauer and A. Dreuw, “Perturbation theoretical approaches to strong light–matter coupling in ground and excited electronic states for the description of molecular polaritons,” *J. Chem. Phys.* **158**, 124128 (2023).

³⁴J. McTague and J. J. Foley, “Non-Hermitian cavity quantum electrodynamics–configuration interaction singles approach for polaritonic structure with *Ab initio* molecular Hamiltonians,” *J. Chem. Phys.* **156**, 154103 (2022).

³⁵F. Pavošević and A. Rubio, “Wavefunction embedding for molecular polaritons,” *J. Chem. Phys.* **157**, 094101 (2022).

³⁶Z.-H. Cui, A. Mandal, and D. R. Reichman, “Variational Lang–Firsov Approach Plus Møller–Plesset Perturbation Theory with Applications to Ab Initio Polariton Chemistry,” *J. Chem. Theory Comput.* **20**, 1143–1156 (2024).

³⁷S. J. Cotton and W. H. Miller, “Symmetrical Windowing for Quantum States in Quasi-Classical Trajectory Simulations,” *J. Phys. Chem. A* **117**, 7190–7194 (2013).

³⁸W. H. Miller, “The Semiclassical Initial Value Representation: A Potentially Practical Way for Adding Quantum Effects to Classical Molecular Dynamics Simulations,” *J. Phys. Chem. A* **105**, 2942–2955 (2001).

³⁹M. Sukharev and A. Nitzan, “Optics of exciton-plasmon nanomaterials,” *J. Phys. Condens. Matter* **29**, 443003 (2017).

⁴⁰C. M. Bustamante, E. D. Gadea, A. Horsfield, T. N. Todorov, M. C. González Lebrero, and D. A. Scherlis, “Dissipative Equation of Motion for Electromagnetic Radiation in Quantum Dynamics,” *Phys. Rev. Lett.* **126**, 087401 (2021).

⁴¹N. Tancogne-Dejean and et al., “Octopus, a computational framework for exploring light-driven phenomena and quantum dynamics in extended and finite systems,” *J. Chem. Phys.* **152**, 124119 (2020).

⁴²S. Yamada, M. Noda, K. Nobusada, and K. Yabana, “Time-dependent density functional theory for interaction of ultrashort light pulse with thin materials,” *Phys. Rev. B* **98**, 245147 (2018).

⁴³H. Chen, J. M. McMahon, M. A. Ratner, and G. C. Schatz, “Classical Electrodynamics Coupled to Quantum Mechanics for Calculation of Molecular Optical Properties: a RT-TDDFT/FDTD Approach,” *J. Phys. Chem. C* **114**, 14384–14392 (2010).

⁴⁴H.-T. Chen, T. E. Li, A. Nitzan, and J. E. Subotnik, “Predictive Semiclassical Model for Coherent and Incoherent Emission in the Strong Field Regime: The Mollow Triplet Revisited,” *J. Phys. Chem. Lett.* **10**, 1331–1336 (2019).

⁴⁵T. E. Li, J. E. Subotnik, and A. Nitzan, “Cavity molecular dynamics simulations of liquid water under vibrational ultrastrong coupling,” *Proc. Natl. Acad. Sci. U.S.A.* **117**, 18324–18331 (2020).

⁴⁶X. Li, A. Mandal, and P. Huo, “Cavity frequency-dependent theory for vibrational polariton chemistry,” *Nat. Commun.* **12**, 1315 (2021), publisher: Nature Publishing Group.

⁴⁷T. E. Li, A. Nitzan, and J. E. Subotnik, “Collective Vibrational Strong Coupling Effects on Molecular Vibrational Relaxation and Energy Transfer: Numerical Insights via Cavity Molecular Dynamics Simulations**,” *Angew. Chem. Int. Ed.* **60**, 15533–15540 (2021).

⁴⁸T. E. Li, A. Nitzan, and J. E. Subotnik, “Polariton relaxation under vibrational strong coupling: Comparing cavity molecular dynamics simulations against Fermi’s golden rule rate,” *J. Chem. Phys.* **156**, 134106 (2022).

⁴⁹T. E. Li, A. Nitzan, and J. E. Subotnik, “Energy-efficient pathway for selectively exciting solute molecules to high vibrational states via solvent vibration-polariton pumping,” *Nat Commun* **13**, 4203 (2022), publisher: Nature Publishing Group.

⁵⁰K. Schwennicke, A. Koner, J. B. Pérez-Sánchez, W. Xiong, N. C. Giebink, M. L. Weichman, and J. Yuen-Zhou, “When do molecular polaritons behave like optical filters?” arXiv (2024), 10.48550/arXiv.2408.05036, doi: 10.48550/arXiv.2408.05036.

⁵¹J. Yuen-Zhou and A. Koner, “Linear response of molecular polaritons,” *J. Chem. Phys.* **160**, 154107 (2024).

⁵²Michael Ruggenthaler, M. Ruggenthaler, Johannes Flick, J. Flick, Camilla Pellegrini, C. Pellegrini, Heiko Appel, H. Appel, I. V. Tokatly, I. V. Tokatly, Ángel Rubio, and A. Rubio, “Quantum electrodynamical density-functional theory: Bridging quantum optics and electronic-structure theory,” *Phys. Rev. A* **90**, 012508 (2014), aRXIV_ID: 1403.5541 MAG ID: 2157656450 S2ID: 049529fb098c19e8821f484512c812db166f2d94.

⁵³J. Flick, M. Ruggenthaler, H. Appel, and A. Rubio, “Kohn–Sham approach to quantum electrodynamical density-functional theory: Exact time-dependent effective potentials in real space,” *Proc. Natl. Acad. Sci. U.S.A.* **112**, 15285–15290 (2015).

⁵⁴J. Flick, M. Ruggenthaler, H. Appel, and A. Rubio, “Atoms and molecules in cavities, from weak to strong coupling in quantum-electrodynamics (QED) chemistry,” *Proc. Natl. Acad. Sci. U.S.A.* **114**, 3026–3034 (2017).

⁵⁵Y. Ke and J. O. Richardson, “Quantum nature of reactivity modification in vibrational polariton chemistry,” *J. Chem. Phys.* **161**, 054104 (2024).

⁵⁶M. R. Fiechter, J. E. Runeson, J. E. Lawrence, and J. O. Richardson, “How Quantum is the Resonance Behavior in Vibrational Polariton Chemistry?” *J. Phys. Chem. Lett.* **14**, 8261–8267 (2023).

⁵⁷I. Simkó and N. M. Hoffmann, “Twin Polaritons: Classical versus Quantum Features in Polaritonic Spectra,” *Phys. Rev. Lett.* **135**, 233601 (2025).

⁵⁸M. A. Zeb, P. G. Kirton, and J. Keeling, “Exact States and Spectra of vibrationally Dressed Polaritons,” *ACS Photonics* **5**, 249–257 (2018).

⁵⁹A. Koner and J. Yuen-Zhou, “Hidden nonlinear optical susceptibilities in linear polaritonic spectra,” *Optica* **12**, 1625 (2025).

⁶⁰T. E. Li, Z. Tao, and S. Hammes-Schiffer, “Semiclassical Real-Time Nuclear-Electronic Orbital Dynamics for Molecular Polaritons: Unified Theory of Electronic and Vibrational Strong Couplings,” *J. Chem. Theory Comput.* **18**, 2774–2784 (2022).

⁶¹M. F. Welman, T. E. Li, and S. Hammes-Schiffer, “Light-Matter Entanglement in Real-Time Nuclear–Electronic Orbital Polariton Dynamics,” *J. Chem. Theory Comput.* **21**, 8291–8307 (2025).

⁶²L. Zhao, Z. Tao, F. Pavošević, A. Wildman, S. Hammes-Schiffer, and X. Li, “Real-Time Time-Dependent Nuclear-Electronic Orbital Approach: Dynamics beyond the Born–Oppenheimer Approximation,” *J. Phys. Chem. Lett.* **11**, 4052–4058 (2020).

⁶³S. P. Webb, T. Iordanov, and S. Hammes-Schiffer, “Multiconfigurational nuclear-electronic orbital approach: Incorporation of nuclear quantum effects in electronic structure calculations,” *J. Chem. Phys.* **117**, 4106–4118 (2002).

⁶⁴S. Hammes-Schiffer, “Nuclear–electronic orbital methods: Foundations and prospects,” *J. Chem. Phys.* **155**, 030901 (2021).

⁶⁵This possibility arises from the fact that for an arbitrary quantum mechanical operator \hat{A} , the expectation value $\langle \hat{A}^2 \rangle$ generally does not equal the square of the expectation value $\langle \hat{A} \rangle^2$; in contrast, equality always holds for the corresponding statement in classical mechanics.

⁶⁶E. Epifanovsky and et al., “Software for the frontiers of quantum chemistry: An overview of developments in the Q-Chem 5 package,” *J. Chem. Phys.* **155**, 084801 (2021).

⁶⁷X. Li, S. M. Smith, A. N. Markevitch, D. A. Romanov, R. J. Levis, and H. B. Schlegel, “A time-dependent Hartree–Fock approach for studying the electronic optical response of molecules in intense fields,” *Phys. Chem. Chem. Phys.* **7**, 233–239 (2005).

⁶⁸M. De Santis, L. Storchi, L. Belpassi, H. M. Quiney, and F. Tarantelli, “Py-BERTHART: A Relativistic Real-Time Four-Component TDDFT Implementation Using Prototyping Techniques Based on Python,” *J. Chem. Theory Comput.* **16**, 2410–2429 (2020).

⁶⁹T. H. Dunning, “Gaussian basis sets for use in correlated molecular calculations. I. The atoms boron through neon and hydrogen,” *J. Chem. Phys.* **90**, 1007–1023 (1989).

⁷⁰Y. Yang, K. R. Brorsen, T. Culpitt, M. V. Pak, and S. Hammes-Schiffer, “Development of a practical multicomponent density functional for electron-proton correlation to produce accurate proton densities,” *J. Chem. Phys.* **147**, 114113 (2017).

⁷¹C. Lee, W. Yang, and R. G. Parr, “Development of the Colle-Salvetti correlation-energy formula into a functional of the electron density,” *Phys. Rev. B* **37**, 785–789 (1988).

⁷²A. D. Becke, “A new inhomogeneity parameter in density-functional theory,” *J. Chem. Phys.* **109**, 2092–2098 (1998).

⁷³A. D. Becke, “Density-functional exchange-energy approximation with correct asymptotic behavior,” *Phys. Rev. A* **38**, 3098–3100 (1988).

⁷⁴K. R. Brorsen, Y. Yang, and S. Hammes-Schiffer, “Multicomponent Density Functional Theory: Impact of Nuclear Quantum Effects on Proton Affinities and Ge-

ometries,” *J. Phys. Chem. Lett.* **8**, 3488–3493 (2017).

⁷⁵J. J. Goings, P. J. Lestrage, and X. Li, “Real-time time-dependent electronic structure theory,” *WIREs Comput Mol Sci* **8**, e1341 (2018).

Supplementary Material

Initialization with a Fock State Cavity Mode in Real-Time Nuclear–Electronic Orbital Polariton Dynamics

Millan F. Welman and Sharon Hammes-Schiffer*

Department of Chemistry, Princeton University, Princeton, NJ 08544

E-mail: shs566@princeton.edu

Contents

1 Q-Chem Input File for HCN with fq-RT-NEO	S3
2 fq-RT-NEO Results for $\mu_{n,x}^n(t)$, $n = 1, \dots, 8$	S7
3 Fourier Transform of $\mu_{n,x}^2(t)$	S8
4 Evaluation of $[\hat{H}, \hat{\mu}^2]$ with Fermionic Operators	S9
References	S11

1 Q-Chem Input File for HCN with fq-RT-NEO

HCN.in_fq for Fig. 5

```
$molecule
0 1
C 0.0 0.0 -0.5026771429
N 0.0 0.0  0.6555628571
H 0.0 0.0 -1.5728771429
$end

$rem
sym_ignore = 1
input_bohr = false
method = b3lyp
neo = true
neo_epc = epc172
basis = cc-pvdz
SCF_ALGORITHM = GDM
thresh = 14
s2thresh = 12
SCF_CONVERGENCE = 11
NEO_N_SCF_CONVERGENCE = 11
MAX_SCF_CYCLES = 500
NEO_PURECART = 1111
NEO_E_CONV = 12
MEM_TOTAL = 7000
NEO_VPP = 0
NEO_BASIS_LIN_DEP_THRESH = 8
$end

$neo_basis
H    3
S    1    1.000000
```

2.828400 1.0
S 1 1.000000
4.0 1.0
S 1 1.000000
5.6569 1.0
S 1 1.000000
8.0 1.0
S 1 1.000000
11.3137 1.0
S 1 1.000000
16.0 1.0
S 1 1.000000
22.6274 1.0
S 1 1.000000
32.0 1.0
P 1 1.000000
2.828400 1.0
P 1 1.000000
4.0 1.0
P 1 1.000000
5.6569 1.0
P 1 1.000000
8.0 1.0
P 1 1.000000
11.3137 1.0
P 1 1.000000
16.0 1.0
P 1 1.000000
22.6274 1.0
P 1 1.000000
32.0 1.0
D 1 1.000000
2.828400 1.0

```

D      1      1.000000
      4.0 1.0

D      1      1.000000
      5.6569 1.0

D      1      1.000000
      8.0 1.0

D      1      1.000000
      11.3137 1.0

D      1      1.000000
      16.0 1.0

D      1      1.000000
      22.6274 1.0

D      1      1.000000
      32.0 1.0

$end

```

```

$neo_tdk

dt 0.04

photon_type 2

is_coherent false 1

photon_basis_size 4

maxiter 200000

field_type delta

field_amp 0.001

in_cavity true 0.3475 0 8e-4 1e8

rt_thresh 4

$end

```

The above input file generates the fq-RT-NEO data given in the main text. The `$neo_tdk` section controls the RT-NEO dynamics. “`photon_type`” determines the level of theory used and is set to 2 for the full-quantum fq-RT-NEO method. “`is_coherent`” initializes the cavity

mode in a coherent state and is set to “false” for all calculations in this work. “1” specifies that one quantum of energy is to be added to the initial condition of the cavity mode. “*in_cavity true 0.3475 0 8e-4 1e8*” denotes coupling of the molecule to a single-mode cavity with a mode frequency of 0.3475 eV, polarization direction x (0 for x , 1 for y , 2 for z), light–matter coupling $\varepsilon = 8 \times 10^{-4}$ a.u., and cavity lifetime $1/\gamma_c = 1 \times 10^8$ a.u. The large cavity lifetime indicates that cavity loss is negligible in these simulations. Finally, “*rt_thresh*” sets the threshold of the real-time predictor-corrector algorithm to 10^{-4} ; this is the *eps* parameter in Algorithm 1 of Ref. S1. All other parameters are assumed to be self-explanatory.

2 fq-RT-NEO Results for $\mu_{n,x}^n(t)$, $n = 1, \dots, 8$

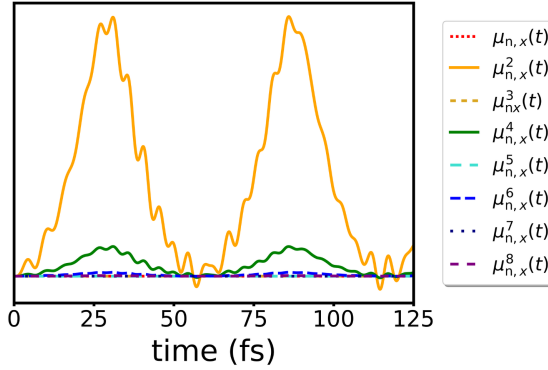


Figure S1: fq-RT-NEO dynamics of $\mu_{n,\lambda}^n(t)$ for $n = 1, \dots, 8$ for HCN. No units are given on the y -axis because these observables have different units.

Figure S1 shows the fq-RT-NEO dynamics of the expectation values of $\mu_{n,\lambda}^n(t) \equiv \text{Tr}[\mathbf{P}_n(t)\boldsymbol{\mu}_{n,\lambda}^n] - \text{Tr}[\mathbf{P}_n(0)\boldsymbol{\mu}_{n,\lambda}^n]$ for $n = 1 \dots 8$. The expectation values for $\mu_{n,\lambda}^2(t)$ and $\mu_{n,\lambda}^4(t)$ are clearly nonzero, oscillating with a slow period of ~ 59 fs and a fast oscillation period of ~ 6 fs. The latter period roughly corresponds to half the period of the oscillations of the free cavity mode, $2\pi/\omega_c = 12$ fs. The expectation values for odd n are all negligible, consistent with the arguments for the model system discussed in the main text.

3 Fourier Transform of $\mu_{n,x}^2(t)$

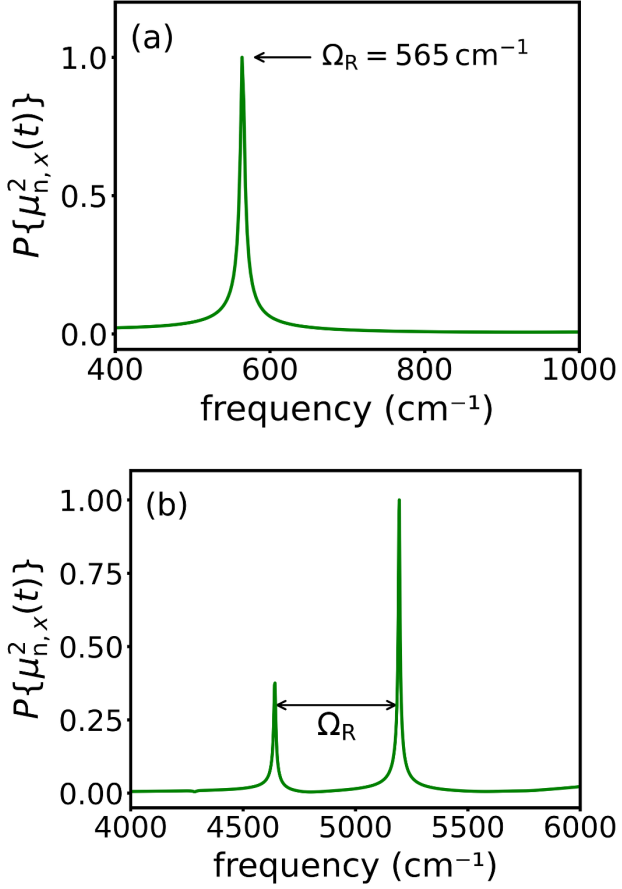


Figure S2: Fourier transform of $\mu_{n,\lambda}^2(t)$ obtained with fq-RT-NEO dynamics applied to HCN for the (a) $400 - 1000 \text{ cm}^{-1}$ region and (b) $4000 - 6000 \text{ cm}^{-1}$ region. In both spectra, the largest signal amplitude has been scaled to a value of 1.

Figure S2a shows the Fourier transform of $\mu_{n,\lambda}^2(t)$ in the region of $400 - 1000 \text{ cm}^{-1}$. A single peak at 565 cm^{-1} matches the peak interpreted as Ω_R and shown in Figure 2a in the main text. Figure S2b shows the Fourier transform of $\mu_{n,\lambda}^2(t)$ in the region of $4000 - 6000 \text{ cm}^{-1}$. A pair of peaks is separated by almost exactly Ω_R and centered at 4918 cm^{-1} , which is redshifted from $2\omega = 5606 \text{ cm}^{-1}$ by $\sim 12\%$. These results are in qualitative agreement with the three-level model presented at the end of the Discussion in the main text.

4 Evaluation of $[\hat{H}, \hat{\mu}^2]$ with Fermionic Operators

We will evaluate $[\hat{H}, \hat{\mu}^2]$, where the dipole operator $\hat{\mu}$ is given by

$$\hat{\mu} = \mu_0(\hat{c}^\dagger + \hat{c}) \quad (\text{S1})$$

and the Hamiltonian \hat{H} is given by

$$\begin{aligned} \hat{H} &= \hat{H}_F + \hat{H}_M + \varepsilon \hat{q} \hat{\mu} \\ &= \hat{H}_F + \hat{H}_M + \varepsilon q_0(\hat{a}^\dagger + \hat{a})\mu_0(\hat{c}^\dagger + \hat{c}) \\ &= \omega \hat{a}^\dagger \hat{a} + \omega \hat{c}^\dagger \hat{c} + g(\hat{a}^\dagger + \hat{a})(\hat{c}^\dagger + \hat{c}). \end{aligned} \quad (\text{S2})$$

Eq. S2 is identical to Eq. 17 in the main text, except that the bosonic annihilation (creation) operator \hat{b} (\hat{b}^\dagger) has been replaced by the fermionic annihilation (creation) operator \hat{c} (\hat{c}^\dagger). To evaluate the commutator, we first invoke the Jacobi Identity

$$[\hat{H}, \hat{\mu}^2] = [\hat{H}, \hat{\mu}] \hat{\mu} + \hat{\mu} [\hat{H}, \hat{\mu}]. \quad (\text{S3})$$

We then evaluate $[\hat{H}, \hat{\mu}]$ using the fermionic commutation relation $[\hat{c}, \hat{c}^\dagger] = 1 - 2\hat{c}^\dagger \hat{c}$, as well as Eqs. S1 and S2:

$$\begin{aligned} [\hat{H}, \hat{\mu}] &= \omega \mu_0 [\hat{c}^\dagger \hat{c}, (\hat{c}^\dagger + \hat{c})] \\ &= \omega \mu_0 (\hat{c}^\dagger \hat{c} \hat{c}^\dagger - \hat{c}^\dagger \hat{c}^\dagger \hat{c} + \hat{c}^\dagger \hat{c} \hat{c} - \hat{c} \hat{c}^\dagger \hat{c}) \\ &= \omega \mu_0 (\hat{c}^\dagger (1 - 2\hat{c}^\dagger \hat{c}) - (1 - 2\hat{c}^\dagger \hat{c}) \hat{c}) \\ &= \omega \mu_0 (\hat{c}^\dagger - 2\hat{c}^\dagger \hat{c}^\dagger \hat{c} - \hat{c} + 2\hat{c}^\dagger \hat{c} \hat{c}). \end{aligned} \quad (\text{S4})$$

In a minimal two-level basis, terms with two consecutive creation or annihilation operators

are equal to the zero operator and can be eliminated, leading to

$$[\hat{H}, \hat{\mu}] = \omega\mu_0 (\hat{c}^\dagger - \hat{c}). \quad (\text{S5})$$

Substituting Eq. S5 into Eq. S3, we obtain the final result:

$$[\hat{H}, \hat{\mu}^2] = \omega\mu_0^2 [(\hat{c}^\dagger - \hat{c})(\hat{c}^\dagger + \hat{c}) + (\hat{c}^\dagger + \hat{c})(\hat{c}^\dagger - \hat{c})] = 2\omega\mu_0^2 (\hat{c}^\dagger \hat{c}^\dagger - \hat{c} \hat{c}). \quad (\text{S6})$$

This is equivalent to Eq. 35 in the main text, with $\hat{b} \rightarrow \hat{c}$. It therefore follows that $[\hat{H}, \hat{\mu}^2] = 0$ within a minimal two-level basis for both fermionic and bosonic molecular systems.

References

[S1] De Santis, M.; Storchi, L.; Belpassi, L.; Quiney, H. M.; Tarantelli, F. PyBERTHART: A Relativistic Real-Time Four-Component TDDFT Implementation Using Prototyping Techniques Based on Python. *J. Chem. Theory Comput.* **2020**, *16*, 2410–2429.